

Sandia National Laboratories
Waste Isolation Pilot Plant

Experimental Work Conducted on MgO Characterization and Hydration

Milestone Report


Haoran Deng,¹ Yongliang Xiong,¹ and Martin Nemer²

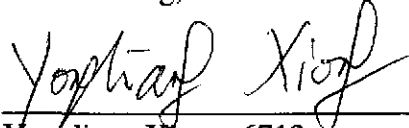
1. Repository Performance Dept. 6712
 2. Performance Assessment and Decision Analysis Dept. 6711
- Sandia National Laboratories
Carlsbad Programs Group
Carlsbad, NM 88220


WIPP:1.4.1.2:PA:QA-L:543261

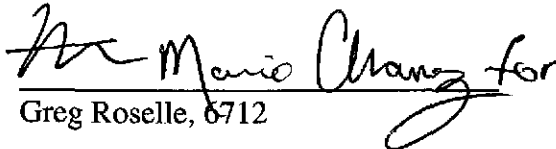
Information Only

APPROVAL PAGE

Author:  8/7/07
Haoran Deng, 6712 Date

Author:  08/07/07
Yongliang Xiong, 6712 Date

Author:  8/7/07
Martin Nemer, 6711 Date

Technical Reviewer: ^{MA}  for 8/7/07
Greg Roselle, 6712 Date

QA Reviewer:  8/7/07
Mario J. Chavez, 6710 Date

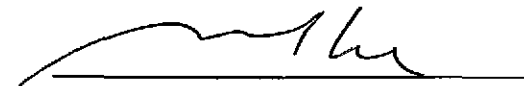
Management Reviewer:  8/07/07
Moo Lee, 6711 Date

TABLE OF CONTENTS

APPROVAL PAGE.....	2
TABLE OF CONTENTS.....	3
LIST OF TABLES.....	5
LIST OF FIGURES.....	6
1 INTRODUCTION.....	8
2 NOMENCLATURE.....	9
3 CHARACTERIZATION.....	10
3.1 Particle Size and Morphology.....	11
3.2 Chemical Analysis of the Composition of MM MgO.....	13
3.3 Loss on Ignition and Thermal Gravimetric Analyses of Hydrated MM MgO.....	14
3.4 Qualitative Chemical Analyses of MM MgO.....	15
4 CALCULATION OF THE MOLE PERCENT PERICLASE IN MM MgO.....	22
4.1 Calculation Methodology.....	23
4.2 Calculation Results.....	26
5 ACCELERATED INUNDATED HYDATATION.....	28
5.1 Container Selection.....	28
5.2 Tracer Dyes.....	29
5.3 Experiment Matrix.....	30
5.4 Factors Influencing the Hydration Rate.....	33
5.5 Volume Change upon Hydration.....	40
5.6 Hydration Mechanisms.....	41

5.7 Comparison with Theoretical Models.....	52
5.7.1 Background on Models.....	52
5.7.2 Modeling Results	53
6 CONCLUSIONS.....	55
7 REFERENCES	56
APPENDIX A. Calculations in the 90-922 Results Spreadsheet	59
APPENDIX B. Experimental Protocol.....	60
B.1 Dissolution of MM MgO in Nitric Acid	60
B.2 TGA and LOI Analysis	61

LIST OF TABLES

Table 1.	Certificate of Analysis for Lot SL2980076 MM MgO.....	10
Table 2.	Typical Bulk Composition of MagChem 10. ¹	11
Table 3.	MgO Size Distribution by Sieving. ¹	12
Table 4.	Concentration of MgO, CaO, Al ₂ O ₃ , Fe ₂ O ₃ , and SiO ₂ in MM MgO (wt %) ¹	14
Table 5.	Weight Lost during TGA and LOI Analyses (wt %).	15
Table 6.	Total Carbon in MM MgO Before and After Hydration (wt %).	15
Table 7.	Impurity Phases Assumed to Be Present in MM MgO.....	23
Table 8.	Concentration of Periclase and Lime in Dry, Unhydrated MM MgO (mol %).	26
Table 9.	Concentration of Periclase and Lime in Dry, Unhydrated MM MgO (wt %).	27
Table 10.	Accelerated, Inundated Hydration Experimental Matrix.....	31
Table 11.	Minitab Report on Hydration Rate and Reaction Factors.....	39
Table 12.	R ² Values for Linear Regression of MM MgO Hydration in DI Water at 70 °C with the Four Models.....	54

LIST OF FIGURES

Figure 1. Particle size distribution by vol %, for particles below 500 μm	13
Figure 2. SEM image (top) and EDS spectrum (bottom) of as-received MM MgO.....	17
Figure 3. SEM image (top) and EDS spectrum (bottom) of a piece of unusual as-received MM MgO.....	18
Figure 4. Low (top left) and high (top right) magnification SEM images and associated EDS spectrum (bottom) of a particle that remained after dissolving the MM MgO in nitric acid.....	19
Figure 5. SEM image (top) and associated EDS spectrum (bottom) of a particle that remained after dissolving the MM MgO in nitric acid.	20
Figure 6. SEM image (top) and associated EDS spectrum (bottom) of a particle that remained after dissolving the MM MgO in nitric acid..	21
Figure 7. Image of dye penetration test.....	29
Figure 8. MM MgO hydration progress (W) versus time (days) for experiments carried out in DI water at 70 $^{\circ}\text{C}$ in an oven (not shaken).	34
Figure 9. Same as Figure 8 for experiments carried out in water bath shaker at 70 $^{\circ}\text{C}$ at a shaking speed of 150 rpm.	35
Figure 10. MM MgO hydration progress (W) versus time (days) for experiments carried out in DI water at 70 $^{\circ}\text{C}$ with big particles.....	36
Figure 11. Same as Figure 10 for experiments carried out in water bath shaker at 70 $^{\circ}\text{C}$ at a shaking speed of 150 rpm, with small particles.....	37
Figure 12. Digital pictures of MM MgO accelerated hydration in DI water at 70 $^{\circ}\text{C}$. The pictures were taken on the 9 th day of hydration.....	41

Figure 13. Image of small-particle size sample before hydration.....	43
Figure 14. Image of small-particle-size sample after 1 day hydration at 70 °C in DI water in the oven.....	44
Figure 15. Image of small-particle-size sample after 9 days of hydration at 70 °C in DI water.....	45
Figure 16. Image of small-particle-size sample after 43 days of hydration at 70 °C in DI water.....	46
Figure 17. Same as Figure 13 at higher magnification.....	47
Figure 18. Same as Figure 14 at higher magnification.....	48
Figure 19. Same as Figure 15 at higher magnification.....	49
Figure 20. Same as Figure 16 at higher magnification.....	50
Figure 21. Hexagonal crystals formed after 26 day of hydration of MM MgO.....	51

1 INTRODUCTION

Magnesium oxide (MgO) is being emplaced in the WIPP as an engineered barrier to mitigate the effects of microbial carbon dioxide (CO₂) generation on actinide mobilities in the postclosure repository environment (Bynum, 1997; Krumhansl, 1997; Bynum et al., 1998; Papenguth et al., 1998). MgO will sequester CO₂ and consume water in brine or water vapor in the gaseous phase. A series of experiments have been conducted at Sandia National Laboratories (SNL) to verify the efficacy of MgO from Martin Marietta Magnesia Specialties LLC. (Martin Marietta) under a test plan (Deng et al., 2006). There are three tasks in the test plan: MgO storage and characterization, MgO hydration, and MgO carbonation. Currently MgO storage, characterization, and accelerated inundated hydration have been completed. Experiments on accelerated humid hydration and MgO carbonation with solution-controlled CO₂ partial pressure (pCO₂) have begun and will be reported on in the next milestone report. In this report we present the experimental results from MgO characterization and accelerated inundated hydration.

Currently the EPA requires the emplacement of 1.67 moles of MgO for every mole of consumable carbon in the emplaced cellulose, plastic, and rubber (CPR) materials. On April 10, 2006, a planned change request was submitted to the EPA requesting approval to “emplace 1.2 moles of magnesium oxide (MgO) for every mole of consumable-organic carbon contained in the Waste Isolation Pilot Plant (WIPP)” (Moody, 2006). One objective of this report is to address uncertainties concerning the amount of periclase plus lime in Martin Marietta (MM) MgO. Another is to show that the new material is effective.

The Brine and Gas Flow (BRAGFLO) code, Version 6.0, is now qualified to model MgO hydration (Nemer, 2006a; Nemer, 2006c). In order to use this feature, defensible rates of MgO hydration must be determined for inundated and humid conditions. Because of the long time scales required to completely hydrate the MgO in brine (years), a defensible mechanistic model of MgO hydration must be developed to extrapolate hydration beyond observable time scales. The MgO hydration experiments will provide the hydration rate and model for such an analysis.

It has been previously found (Fernandez et al., 1999) that (a) particle size, (b) solid-to-liquid ratio, and (c) stirring speed all affect the rate of carbonation of MgO slurries. Thus it is reasonable to hypothesize that these factors would also affect the rate of hydration. As described in Subsection 5, accelerated MgO hydration experiments were carried out with two or three levels for each of the above factors in de-ionized (DI) water at 70 °C. The Minitab statistical software package was used to determine the test matrix and analyze the test results. We then fit the accelerated inundated hydration data to four different kinetic models and calculated the hydration rate in Subsection 5.7.

2 NOMENCLATURE

In this report, “MgO” refers to the bulk, granular material being emplaced in the WIPP to serve as the engineered barrier. MgO comprises mostly periclase (pure, crystalline MgO – the main reactive constituent of the engineered barrier), which will consume CO₂ and water (H₂O) and form brucite (Mg(OH)₂), hydromagnesite (Mg₅(CO₃)₄(OH)₂·4H₂O), and eventually magnesite (MgCO₃). The terms “periclase,” “brucite,” “hydromagnesite,” and “magnesite” are mineral names and should, therefore, be restricted to naturally occurring forms of materials that meet all other requirements of the definition of a mineral (see for example, Bates and Jackson, 1984). However, mineral names are used herein for convenience and will be used to referring as individual components of the MM MgO.

3 CHARACTERIZATION

Characterization was performed on a single lot of MM MgO under the test plan of Deng et al. (2006). A manufacturer's analysis sheet (Martin Marietta Magnesia Specialties Inc., 2006a) arrived with this lot of MM MgO. The relevant pieces of information from the analysis sheet are listed below in Table 1.

Table 1. Certificate of Analysis for Lot SL2980076 MM MgO.

Product:	MagChem 10 WTS 60
Plant Shipping No.:	SL2980076
Truck:	156/051506
Magnesium as MgO (on ignited basis) %:	98.39
Loss on Ignition %:	0.22

A typical composition for MagChem 10 (WTS-60 is a grade of MagChem 10) can be obtained from the manufacturer's specifications sheet (Martin Marietta Magnesia Specialties Inc., 2006b), a synopsis of which is given below in Table 2.

Table 2. Typical Bulk Composition of MagChem 10.¹

Constituent Name	Typical (wt %)	Specifications (wt %)
Magnesium oxide (MgO)	98.2	97.0 min
Calcium oxide (CaO)	0.9	1.0 max
Silica (SiO ₂)	0.4	0.5 max
Iron oxide (Fe ₂ O ₃)	0.2	0.3 max
Aluminum oxide (Al ₂ O ₃)	0.1	0.2 max

1. These results are from Martin Marietta's total chemical analysis (Martin Marietta Magnesia Specialties Inc., 2006b). Magnesium, calcium, silica, iron, and aluminum are reported here in terms of the oxides above, which aren't necessarily representative of the actual phases in the MM MgO.

3.1 Particle Size and Morphology

Particle size, intergranular porosity, and fracture topology of the MgO particles may all affect the mass transport of reactants to the unreacted MgO surface, and thus affect the reaction rate. To determine the size distribution as a function of mass fraction, the MM MgO was passed through a series of Fisher Scientific sieves ranging from 75 μm (200 Mesh) to 2.0 mm (10 Mesh), then the fractions between each pair of sieves (or above and below the sieve for the largest and smallest) were collected and weighed. The size distribution obtained is similar to the manufacturer's analysis sheet (2006a) that accompanied this lot of MM MgO. Our results are compared with those of Martin Marietta below in Table 3.

The particle size distribution (by vol %) for particles smaller than 500 μm was determined using a Malvern Instruments Mastersizer laser-scattering particle-size analyzer. The results are shown in Figure 1. The size distribution is clearly multimodal below 500 μm , with peaks at around 0.4 μm , 10 μm , and 500 μm . Looking at the scanning electron microscope (SEM) image in Figure 2, one can understand the source of this multimodal distribution. Martin Marietta MgO is a sintered product consisting of small particles of MgO sintered together to make larger particles. Figure 2 shows that much of this sintered product is made up by $\sim 10 \mu\text{m}$ particles, with smaller flakes filling the interstitial voids.

Table 3. MgO Size Distribution by Sieving.¹

Mesh #	Average (wt %)	Standard Deviation (wt %)	Wt % Passing Through the Sieve ²	Mesh #	Wt % Passing Sieve ³
> 10 (> 2.0 mm)	7.02	0.91	92.98	3/8 inch (9.5 mm)	100
10 - 18 (2.0 mm – 1.0 mm)	32.52	1.76	60.45	6 (3.4 mm)	99.9
18 - 30 (1.0 mm – 600 µm)	20.25	1.28	40.21	16 (1.18 mm)	73.1
30 - 50 (600 µm – 300 µm)	12.74	2.19	27.47	30 (600 µm)	41.6
50 - 100 (300 µm – 150 µm)	5.35	0.70	22.12	100 (150 µm)	21.3
100 - 200 (150 µm – 75 µm)	3.36	0.35	18.77		
< 200 (< 75 µm)	17.91	1.88			
Total	100	0			

1. This data can be found in the Excel spreadsheet MgO size distribution.xls worksheet.
2. The average and standard deviation are based on analyses of 10 bottles of MM MgO.
3. Manufacturer's analysis sheet (2006a).

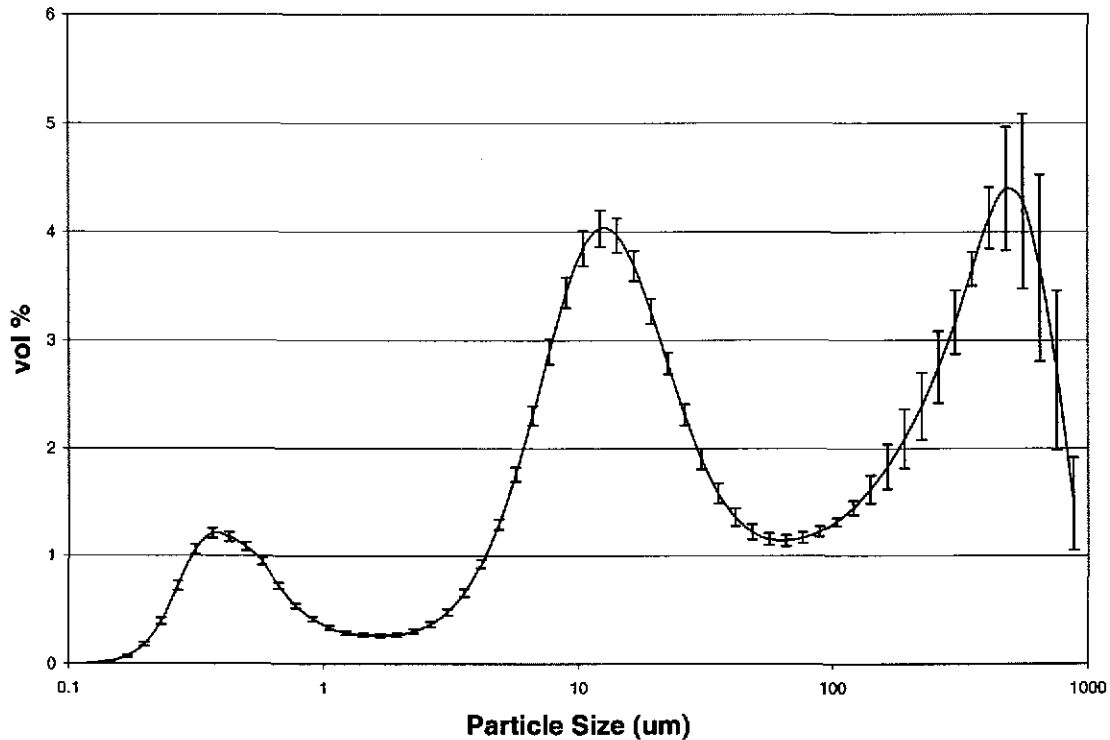


Figure 1. Particle size distribution by vol %, for particles below 500 μm . This data and the calculations associated with it are given in the Microsoft Excel spreadsheet set1-1rall.xls. The curve is the mean of three analyses and the error bars are one standard deviation above and one standard deviation below the mean.

3.2 Chemical Analysis of the Composition of MM MgO

A lower bound on the amount of magnesium, calcium, aluminum, iron, and silicon was determined by SNL by dissolving samples of MM MgO in nitric acid. This is a lower bound because a small fraction of nitric-acid insoluble solids remains after dissolution that was not quantitatively analyzed. The insoluble solids remaining after dissolution amounted to about 0.4 wt % of the MM MgO. The concentrations of calcium, magnesium, aluminum, iron and silica ions in nitric acid are measured by inductively-coupled plasma atomic emission spectrometer (ICP-AES). Table 4 shows the concentration of MgO, CaO, Al₂O₃, Fe₂O₃ and SiO₂ in MM MgO (wt %), see Subsection B.1 of APPENDIX B for the experimental protocol. This data (wt %) can be found on the Mgo-si-sum sheet of the Microsoft Excel file MgO-ICP.xls, cells J15 through N16.

Table 4. Concentration of MgO, CaO, Al₂O₃, Fe₂O₃, and SiO₂ in MM MgO (wt %)¹.

	MgO	CaO	Al ₂ O ₃	Fe ₂ O ₃	SiO ₂	Sum ³
Average ²	98.46	0.87	0.13	0.12	0.31	99.89
Standard Deviation ²	2.54	0.03	0.02	0.01	0.01	2.54

1. MgO, CaO, Al₂O₃, Fe₂O₃, and SiO₂ aren't necessarily representative of the actual phases in the MM MgO.
2. The average and standard deviation are based on 12 analyses.
3. Here Sum is calculated as the summation of the left hand columns, and the standard deviation is calculated using equation 9.

For the purposes of determining a mole percent of periclase in MM MgO, we use the amount of aluminum oxide, iron oxide and silica oxide from Table 4. The amount of potentially reactive lime in the MM MgO is also taken from Table 4. The amount of magnesium oxide reported in Table 4 is the total amount of magnesium oxide, not all of which is periclase in the bulk material. The magnesium oxide result in Table 4 is not used in the calculation of the mole-percent periclase plus lime, calculated in Section 4. As will be described further below in Section 4, to the precision achieved in this analysis, whether the reported calcium oxide is lime or in some other calcium-bearing phase has virtually no impact on the total mole fraction of periclase plus lime.

3.3 Loss on Ignition and Thermal Gravimetric Analyses of Hydrated MM MgO

The weight percent of water driven off from hydrated MM MgO during loss on ignition (LOI) and thermal gravimetric analyses (TGA) is used to determine the amount of magnesium and calcium that are in the phases periclase and lime, respectively. As there are only small amounts of impurities in the MM MgO, the hydration of the impurities is not taken into account. Procedures of LOI and TGA can be found in Subsection B.2 of APPENDIX B.

In this analysis, we prepared samples of MM MgO that were hydrated at 90 °C for at least three days, which converts periclase and lime to brucite and portlandite, respectively. The samples were then dried and subjected to the temperature protocol given above which causes brucite and portlandite to convert to periclase and lime, respectively. These results are given below in Table 5 and are used in Section 4. The results in Table 5 are calculated in the Microsoft Excel spreadsheet 90-922 results 4.xls, on the TGA and LOI sheet, cells B21-B22, where references to the appropriate data sources are given.

Table 5. Weight Lost during TGA and LOI Analyses (wt %).

	Weight Lost (from Hydrated MM MgO) during TGA and LOI Analysis
Average: ¹	29.8946
Standard deviation: ¹	0.3771

1. The average and standard deviation are based on 8 analyses.

To ensure that calcite precipitation did not contribute significantly to the TGA and LOI analyses, we performed a total carbon analysis on MM MgO before and after hydration by carbon coulometry. This analysis was performed under the procedure of Deng (2006). The results are shown below in Table 6. One sample that was re-soaked in de-ionized water (DI water) at room temperature for several days did show calcium carbonation; the results from this sample are not used in this analysis. These results used to produce Table 6 are located in the 90-922 results 4.xls spreadsheet, cells C55, C56, C75, and C76.

Table 6. Total Carbon in MM MgO Before and After Hydration (wt %).

	Average Carbon	Standard Deviation
Dry, unhydrated MM MgO ¹	0.05	0.02
Hydrated MM-MgO ¹	0.07	0.01

1. The average and standard deviation are based on six analyses.

3.4 Qualitative Chemical Analyses of MM MgO

To gain some understanding of the phases present in MM MgO, we took SEM images and associated energy dispersive spectroscopy (EDS) spectra of as-received MM MgO, and of the insoluble portion after dissolution in nitric acid; these analyses followed the procedure of Nemer (2006d). These spectra are located in scientific notebook supplemental binders WIPP-MM MgO-2 SEM/EDS supplemental binder-1 and WIPP-MM MgO-4 SEM/EDS supplemental binder-1, which are associated with scientific notebooks WIPP-MM MgO-2 and WIPP-MM MgO-4.

SEM images of particles of as received MM MgO and associated EDS spectra are shown in Figure 2 and Figure 3. Figure 2 shows a typical particle of MgO; the large particle is a sintered collection of small particles; the EDS spectrum shows Mg, O, and a small amount of Ca. Figure 3 shows an unusual particle; the EDS spectrum of shows Mg, Ca, Si, Fe, and O.

Images of the particles that remained after dissolving the MM MgO in nitric acid are shown in Figure 4, Figure 5 and Figure 6. Figure 4 shows a particle that contains Fe, O and lesser amounts of other elements. This particle appears to be some kind of iron oxide, perhaps hematite. The iron oxide may have come from the brine from which the MgO is obtained or it may have come from the processing equipment. Figure 5 shows a particle that contains Mg, Al, Fe, Cr, and O. This particle is most likely a spinel or a solid solution of several spinels, such as those listed in Table 7. Spinel forms when MgO fuses with the oxides of aluminum, iron, or chromium at high temperature (Deer et al., 1992). The chromium most likely came from the steel equipment used to burn the MgO at high temperature. Spinel may have formed during the high-temperature burn, or (non-chromium spinel) may have formed naturally in the magnesium deposits from which the magnesium is mined. Figure 6 shows what may be a particle of MgO that did not completely dissolve in nitric acid. We suspect that the appearance of particles of MgO, as shown in Figure 6, are an artifact of incomplete acid digestion, as it appears from Figure 6 that the acid had partially etched its surface (compare Figure 2 to Figure 6).

Little Si and Ca were found in the nitric-acid insoluble particles. For silica, this may be because the nitric acid-MgO mixture heats-up during the digestion due to the enthalpy of the nitric acid-MgO reaction. Silicon dioxide may gel when heated in nitric acid (Kolthoff et al., 1962). Some of the gel may have been rinsed away when filtering the particles.

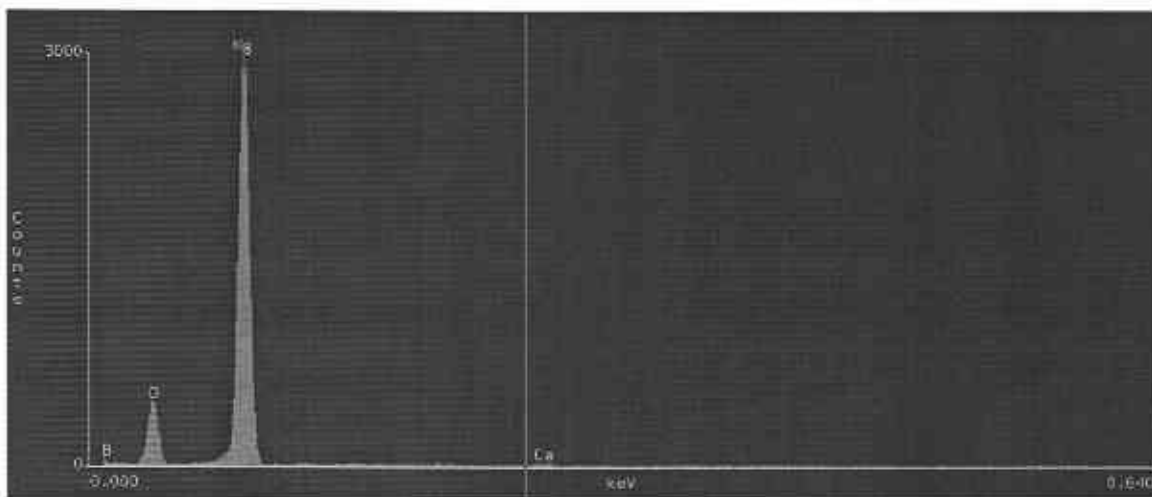
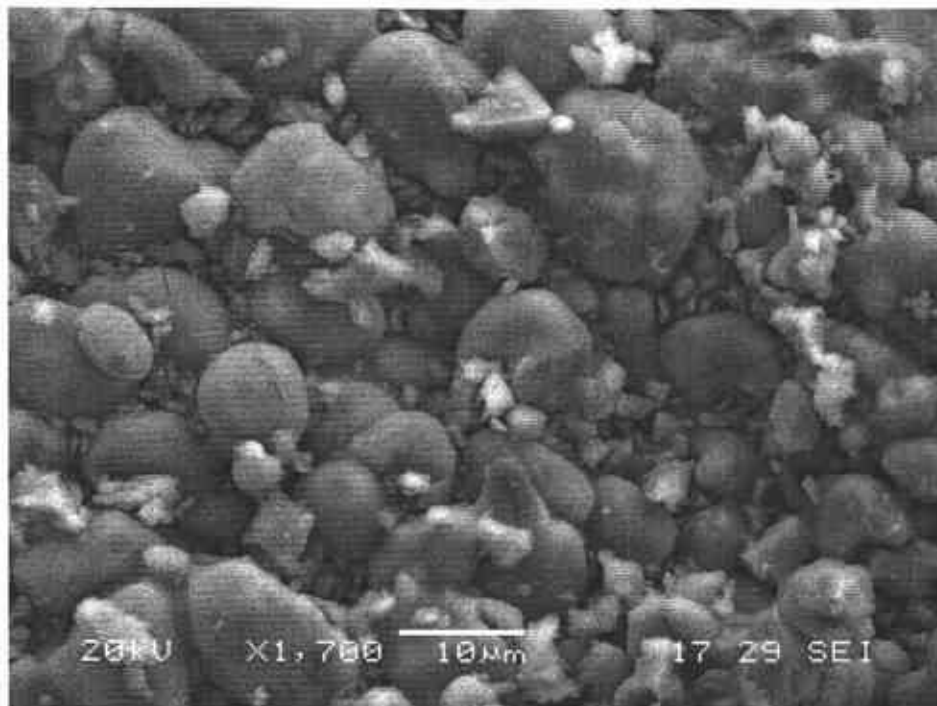


Figure 2. SEM image (top) and EDS spectrum (bottom) of as-received MM MgO. Small amounts of calcium are evident from the EDS spectrum. The SEM image is stored in the file 816h4i2a.bmp; the EDS spectrum is stored in 816h4i2a.eda. Both are located in: WIPP-MM MgO-2 SEM/EDS supplemental binder-1.

Information Only



Figure 3. SEM image (top) and EDS spectrum (bottom) of a piece of unusual as-received MM MgO. Gold is from Au-Pd coating prior to imaging, carbon is from the carbon tape mount. The SEM image is stored in the file 816h4i2a.bmp; the EDS spectrum is in 816h4i2a.eds. Both are located in: WIPP-MM MgO-2 SEM/EDS supplemental binder-1.

Information Only

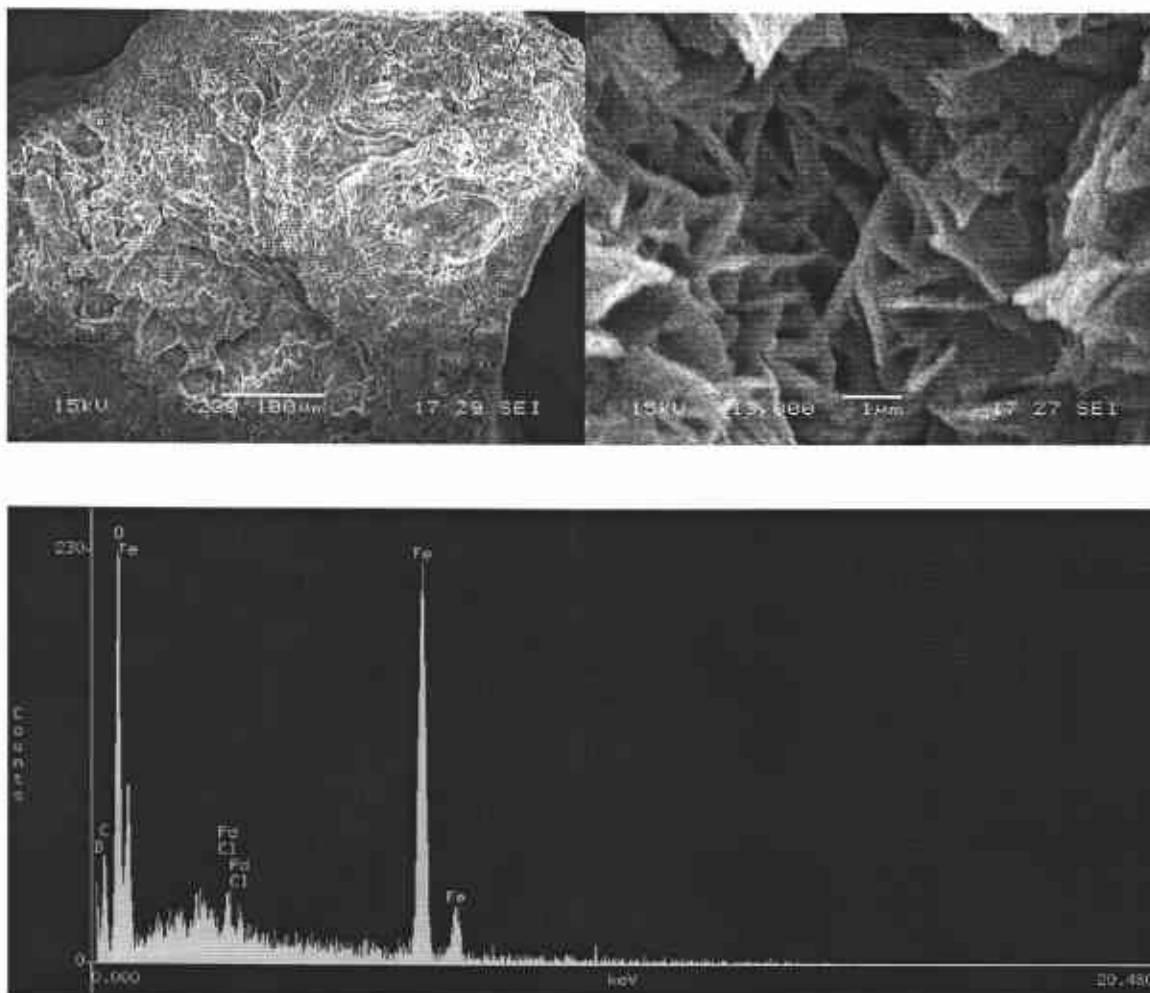


Figure 4. Low (top left) and high (top right) magnification SEM images and associated EDS spectrum (bottom) of a particle that remained after dissolving the MM MgO in nitric acid. Palladium is from Au-Pd coating prior to imaging, C is from the carbon tape mount. The first SEM image is stored in the file 718h1i2.bmp; the second is stored in the file 718h1i4.bmp; the EDS spectrum is in 718h1i4s1.eds. All are located in: WIPP-MM MgO-2 SEM/EDS supplemental binder-1.

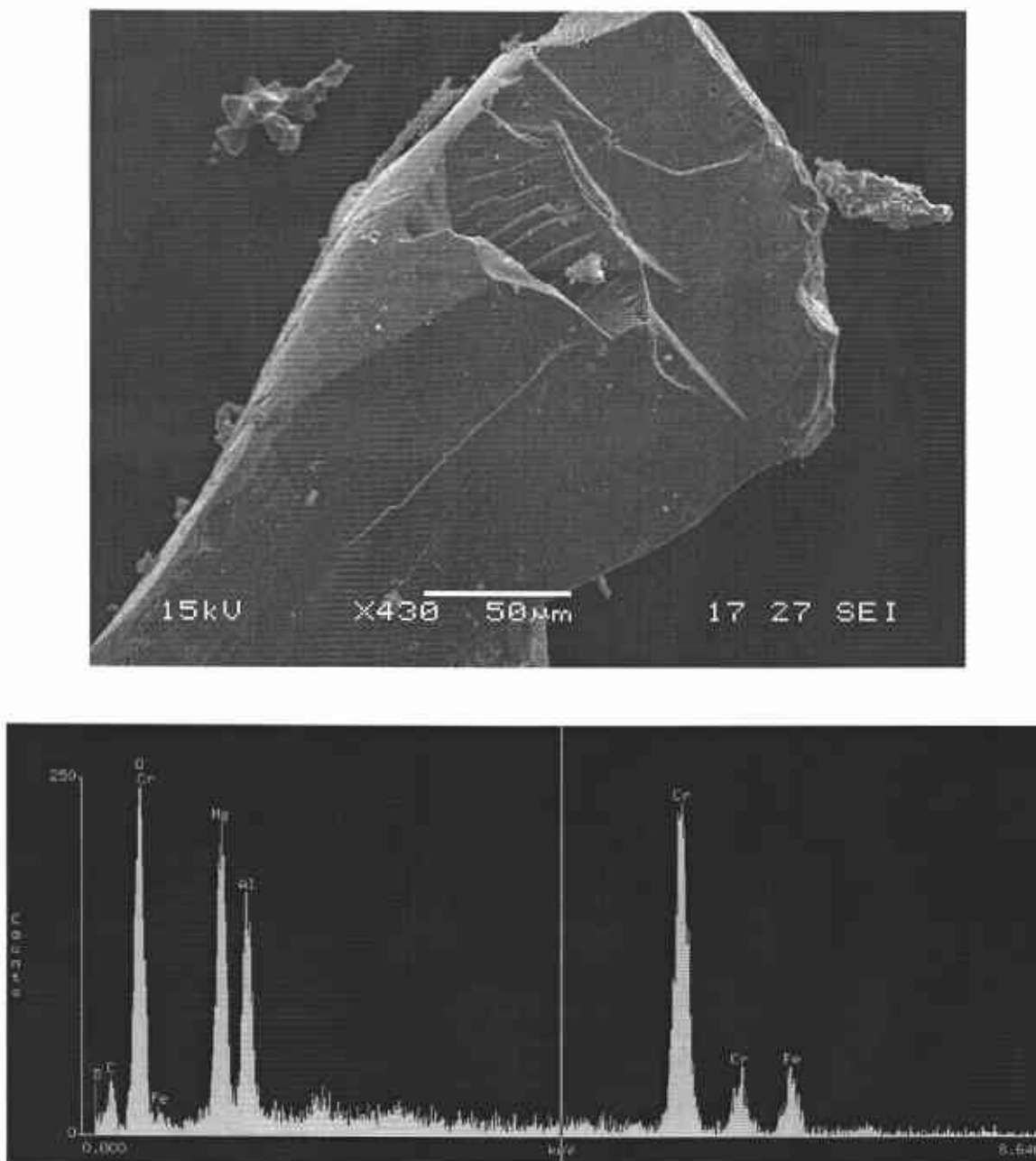


Figure 5. SEM image (top) and associated EDS spectrum (bottom) of a particle that remained after dissolving the MM MgO in nitric acid. Notice the conchoidal fractures in the SEM image; spinels generally lack cleavage (Deer et al., 1992). The SEM image is stored in the file 718h1i5a.bmp; the EDS spectrum is in 718h1i5as1.eds. Both are located in: WIPP-MM MgO-2 SEM/EDS supplemental binder-1.

Information Only

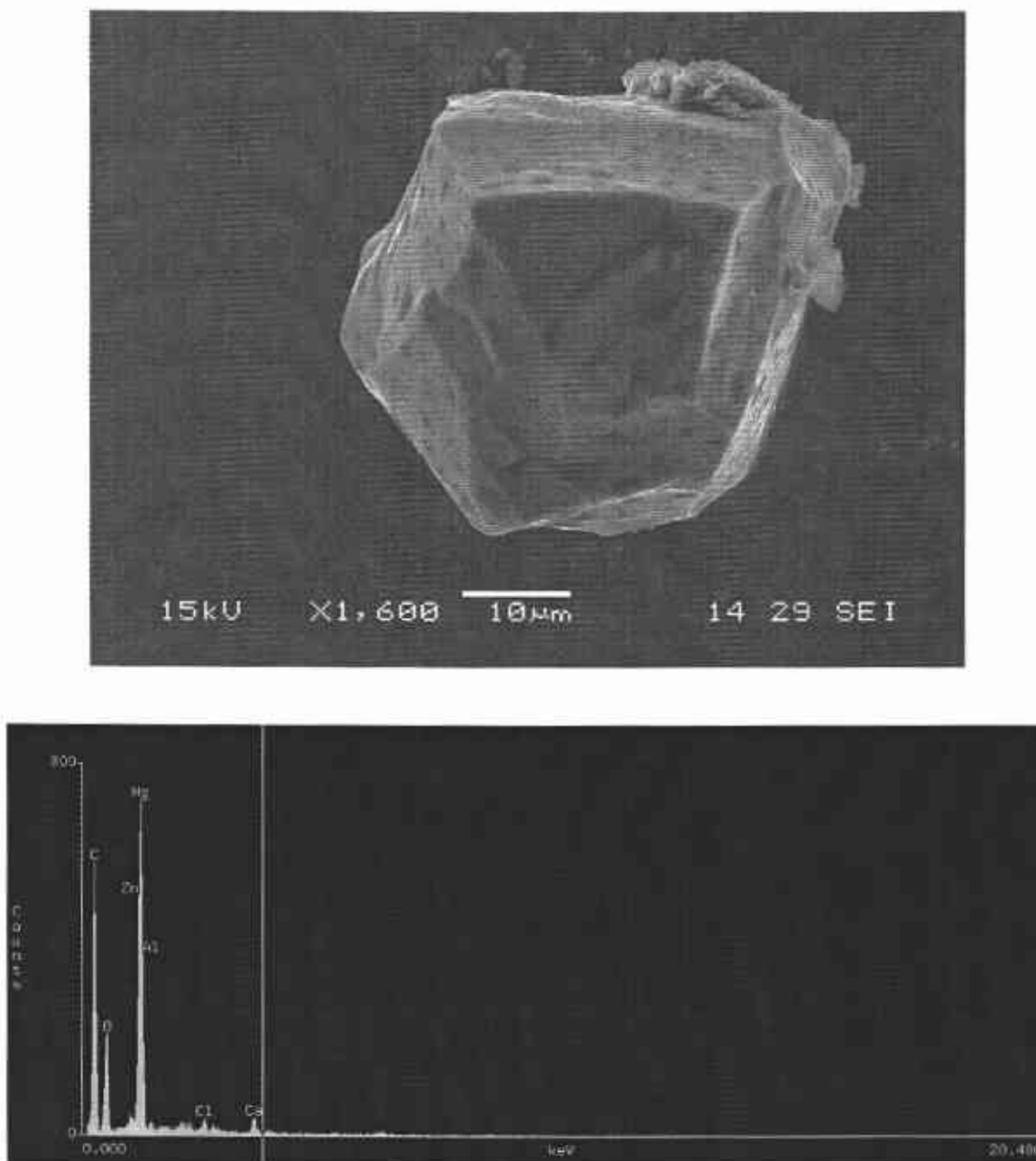


Figure 6. SEM image (top) and associated EDS spectrum (bottom) of a particle that remained after dissolving the MM MgO in nitric acid. The SEM image is stored in the file 123h1i10.bmp; the EDS spectrum is in 1023h1i10.eds. Both are located in: WIPP-MM MgO-4 SEM/EDS supplemental binder-1.

Information Only

4 CALCULATION OF THE MOLE PERCENT PERICLASE IN MM MgO

In this section we calculate a mole fraction of periclase plus lime in MM MgO. This is accomplished by calculating the moles of water of hydration that were released from the MM MgO during TGA and LOI analyses, and by making educated assumptions on the likely impurity phases.

To determine the mole fraction of periclase and lime (the principal constituents of MM MgO), the following assumptions were made:

- (a) Any unbound water was lost at temperatures below 150 °C.
- (b) Water lost between heating hydrated MM MgO to 800 °C and 150 °C from TGA and LOI experiments (given in Table 5) came from brucite and portlandite. Because the decomposition temperatures of brucite (350-800 °C) and portlandite (450-800 °C) (see p A9 of supplemental binder WIPP-MM MgO-4 TGA supplemental binder, for portlandite see also Alarcon-Ruiz et al., 2005) overlap (at least under the conditions used), we found it difficult to separate out the water from the two compounds.
- (c) Most of the calcium in Table 4 is lime that reacts with water to form portlandite. It is important to note that, to the precision achieved in this analysis, this assumption has virtually no impact on the total mole fraction of periclase + lime; it only affects how the moles of H₂O (lost during TGA and LOI experiments) are divided up between periclase and lime.
- (d) Based on the images, spectra, and discussion in Subsection 3.4, we believe that the impurity portion of as-received MM MgO consists of SiO₂, perhaps olivines or orthosilicates, hematite, minerals in the spinel group and/or solid solutions of various spinels, and perhaps small amounts of MgO that were occluded in various impurity phases. A subset of the phases considered to be representative of the impurity material is listed below in Table 7. However, given that we do not know quantitatively how the mass of impurity material is distributed among the various impurity phases, in this preliminary analysis we assign all of the aluminum to alumina and all of the iron to hematite,

$$x_{Al_2O_3} = \frac{1}{2} x_{Al} \quad (1)$$

$$x_{Fe_2O_3} = \frac{1}{2} x_{Fe} \quad (2)$$

Here x_i is the moles of phase (or element) i per gram of dry, unhydrated sample. The moles of iron oxide and aluminum oxide per gram of dry sample were determined by dividing the mean results in Table 4 by their respective molecular weights. Assumptions 1 and 2 will be shown in

Subsection 4.2 to be representative of a lower bound on the mole fraction of periclase, assuming that the phases in Table 7 are representative.

Table 7. Impurity Phases Assumed to Be Present in MM MgO, in Order of Molecular Weight.

Mineral or Oxide	Chemical Formula	Molecular Weight (g/mol)
Silica	SiO ₂	60.084
Alumina	Al ₂ O ₃	101.960
Spinel	MgAl ₂ O ₄	142.265
Hematite	Fe ₂ O ₃	159.692
Hercynite	FeAl ₂ O ₄	173.807
Magnesiochromite	MgCr ₂ O ₄	192.293
Chromite	FeCr ₂ O ₄	223.837

4.1 Calculation Methodology

The mole fractions of periclase and lime ($X_{\text{periclase}}$ and X_{lime} , respectively) are calculated by,

$$X_{\text{periclase}} = \frac{x_{\text{periclase}}}{\sum_i x_i}, \quad (3)$$

$$X_{\text{lime}} = \frac{x_{\text{lime}}}{\sum_i x_i}. \quad (4)$$

where i is an index for periclase, lime, SiO₂, Al₂O₃, Fe₂O₃, and other. The phases considered to be contributing to Equations 3–4 are: periclase, lime, SiO₂ (of unknown phase), alumina (Al₂O₃), and hematite (Fe₂O₃). The index “other” represents the moles of impurity material other than SiO₂, Al₂O₃, and Fe₂O₃. This is discussed further below with Equation 7. The mean moles of silicon per gram of dry, unhydrated sample, x_{Si} , was obtained by dividing the results in Table 4 by the molecular weight of SiO₂.

The amount of periclase in the MM MgO (to be used in Equation 3 above) is equal to the amount of water lost during TGA and LOI analysis minus the amount of lime present

$$x_{\text{periclase}} = x_{\text{H}_2\text{O}} - x_{\text{lime}} \quad (5)$$

where x_{lime} was obtained by dividing the mean weight percent of CaO from Table 4 (see assumptions a-b above) by the molecular weight of lime (CaO), and $x_{\text{H}_2\text{O}}$ is the moles H₂O lost/g dry, unhydrated sample from TGA and LOI analysis, and is calculated from,

$$x_{\text{H}_2\text{O}} = \frac{\text{wt}\%_{\text{lost}} / 100}{1 - \text{wt}\%_{\text{lost}} / 100} \times \frac{1}{\text{MW}_{\text{H}_2\text{O}}} \quad (6)$$

Here $\text{wt}\%_{\text{lost}}$ is the weight percent lost during LOI and TGA experiments, the mean was used and is given in Table 5. The term $(1 - \text{wt}\%_{\text{lost}})$ in the denominator of Equation 6 accounts for the difference between weight percent in the hydrated sample and weight percent in the dry-unhydrated sample. We need to convert to weight percent in the dry-unhydrated sample because the weight percents of CaO, SiO₂, Al₂O₃, and Fe₂O₃ in Table 4 are in terms of the dry, unhydrated sample weight.

For the purpose of calculating a mole fraction, the remaining impurity weight percent (other than periclase, lime, SiO₂, hematite, and alumina) is then assigned to unreacted MgO,

$$x_{\text{other}} = \frac{\left(1 - \sum_i x_i \text{MW}_i\right)}{\text{MW}_{\text{MgO}}}, \quad (7)$$

where MW_i is the molecular weight of species i , and here i is an index for: periclase (from Equation 5), lime (from Table 4 divided by MW_{CaO}), SiO₂ (from Table 4 divided by MW_{SiO_2}), Al₂O₃ (from Equation 1), and Fe₂O₃ (from Equation 2). The calculated x_{other} is thus an upper estimate of the total moles of impurity material (other than Fe₂O₃, Al₂O₃, SiO₂) since the molecular weight of the impurity phases in Table 7 are all larger than that of MgO.

For the purpose of reporting an uncertainty, we used the standard deviations in the experimental measurements to propagate uncertainty through Equations 3-7. Uncertainty in linear equations was propagated using the following standard formulas. Given y , a function of means $\bar{\eta}_i$ of random variables \square_i , and constants a_i and c ,

$$y = \sum_i a_i \bar{\eta}_i + c, \quad (8)$$

then if the uncertainties in \square_i are independent,

$$V_y = \sum_i a_i^2 V_i, \quad (9)$$

where V_y is the variance of the function y and V_i are the variances in the random variables η_i , and if the uncertainties are not independent we use the upper bound

$$\sigma_y = \sum_i |a_i| \sigma_i, \quad (10)$$

where σ_y is the standard deviation of the function y and σ_i are the standard deviations in the functions η_i . Equations 9 and 10 may be found in Taylor (1982), p 56, Equations 3.16 and 3.17. Equations 1-2 are functions of one random variable, hence we used Equation 9. In Equation 7 the uncertainties are not independent and hence we used Equation 10. For other functions of random variables, i.e.,

$$y = f(\bar{\eta}_1, \dots, \bar{\eta}_n), \quad (11)$$

the following rule is used,

$$V_y = \left(\frac{\partial y}{\partial \bar{\eta}_1} \delta \bar{\eta}_1 \right)^2 + \dots + \left(\frac{\partial y}{\partial \bar{\eta}_n} \delta \bar{\eta}_n \right)^2, \quad (12)$$

if the random variables are independent, and we use the upper bound

$$\sigma_y = \left| \frac{\partial y}{\partial \bar{\eta}_1} \right| \sigma_1 + \dots + \left| \frac{\partial y}{\partial \bar{\eta}_n} \right| \sigma_n, \quad (13)$$

if the random variables are correlated. Equations 12 and 13 may be found in Taylor (1982), p 73, Equations 3.47 and 3.48.

In Equation 6 there is only one random variable and hence we use Equation 12, which yields,

$$V_{H_2O} = \left(\frac{\sigma_{wt\%lost} / 100}{\left(1 - \overline{wt\%lost} / 100 \right)^2 MW_{H_2O}} \right)^2. \quad (14)$$

In Equations 3 and 4 the various x_i terms are not independent and hence we use Equation 13 which yields,

$$\sigma_{x_{\text{periclase}}} = \left| \frac{1}{\sum_i \bar{x}_i} - \frac{\bar{x}_{\text{periclase}}}{\left(\sum_i \bar{x}_i\right)^2} \right| \sigma_x + \frac{\bar{x}_{\text{periclase}}}{\left(\sum_j \bar{x}_j\right)^2} \sum_{i \neq x_{\text{periclase}}} \sigma_i, \quad (15)$$

and a similar result for lime (replacing terms labeled MgO with CaO).

4.2 Calculation Results

The results of the calculations described in Subsection 4.1 are given below in Table 8 for the mole fraction of periclase and lime, and Table 9 for the weight fraction of periclase and lime. Equations 3-4 were used to calculate the average mole fraction of periclase and lime, and Equation 15 was used to calculate the standard deviation. For the sum of periclase and lime, the standard deviations were summed (since they are not independent). These calculations are performed in the Microsoft Excel spreadsheet 90-922 results 4.xls (see APPENDIX A). The Reported Value column shows the values that we are reporting.

Table 8. Concentration of Periclase and Lime in Dry, Unhydrated MM MgO (mol %).

	Average	Standard Deviation	Reported Value mean \pm \square
Periclase	95.2	1.82	95 \pm 2
Lime	0.631	0.0405	0.63 \pm 0.04
Periclase + Lime	96.0	1.86	96 \pm 2

Table 9. Concentration of Periclase and Lime in Dry, Unhydrated MM MgO (wt %).

	Average	Standard Deviation	Reported Value mean \pm \square
Periclase	94.8	1.72	95 \pm 2
Lime	0.874	0.0256	0.87 \pm 0.03
Periclase + Lime	95.6	1.74	96 \pm 2

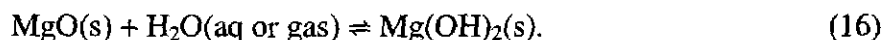
By fitting the unreacted weight percent into phases with lower molecular weights (i.e., SiO₂, Al₂O₃, hematite, and MgO) compared to other possible phases listed in Table 7, we calculated a lower estimate of the periclase mole fraction than if we had assumed species with larger molecular weights such as magnesiochromite and chromite. Although these phases were not confirmed experimentally, chromium was common in the undissolvable portion of the MgO as described above in Subsection 3.4. The weight fraction of periclase in Table 9 is ~ 2% lower than the specification given in Table 2 and 3.5% lower than the result in Table 4 (from the dissolution of MM MgO in nitric acid). One must remember that the MgO reported in Table 2 and Table 4 is not necessarily in the phase periclase. The difference in the results from Table 9 and Table 4 is probably a good upper-bound estimate of the amount of magnesium tied up in impurity phases. This is consistent with the results of Equation 7, which gives the weight fraction of other = 3.4% (see Subsection 4.1); this is calculated in cells T41 in the 90-922 results 4.xls spreadsheet.

Wall (2005) performed a similar analysis on a lot of WTS-30, which was not the same lot analyzed here. In her analysis she found a periclase mole percent of 96 \pm 2.5 (one sigma). In her analysis, she assumed that all of the water lost during LOI came from brucite, and that the remaining weight percent is unreactive MgO. The result obtained by Wall is very close to the result given above in Table 8. This is not surprising since the minor impurity constituents (Fe, Al, Si) given in Table 4 add up to less than 1 wt %, most of which is SiO₂, whose molecular weight is close to that of MgO.

The mole percent of periclase given in Table 8 and Table 9 are equal to within two significant digits. If we had assumed that all of the MM MgO material was either periclase or unreactive MgO (i.e., no Ca, Si, Fe, Al), then the mole fraction and weight fraction would be equal since in that case there would only be a single molecular weight. Because the total weight percent of the other components (Ca, Si, Fe, Al) is small, the contributions of the other components (Ca, Si, Fe, Al) are perturbations on this result, hence the small difference between the weight and mole percent.

5 ACCELERATED INUNDATED HYDRATION

After the WIPP is filled and sealed, the periclase in the MgO emplaced in the repository will react with water in the gas phase or in brine to form brucite



Particle size, solid-to-liquid ratio, and stir speed may all influence MgO hydration kinetics. In order to determine which parameters are most important in determining the MgO hydration and carbonation kinetics, and therefore which should be carefully controlled in long-term experiments, a fractional-factorial (Box et al., 1978) accelerated MgO hydration experiment was carried out with two to three levels for each of the above factors in DI water at 70 °C. We found the MgO particle size is most important factor affecting hydration rate while the solid-to-liquid ratio, and stir speed do not have a significant effect on the hydration rate. We also found that MM MgO hydrated much faster than Premier MgO. In DI water, MM MgO hydrated to 96 mol % brucite in 43 days at 70 °C. Only 80 mol % of Premier MgO hydrated to brucite in 78 days at 70 °C (Snider, 2002).

5.1 Container Selection

The loss of salt and water from the bottles containing brine is a problem in many long-term geochemistry experiments involving brine. In our test plan, experiments with various MgO-to-brine/water ratios are being performed. It is therefore crucial to minimize salt loss and water loss to prevent changing the brine composition and to keep the MgO-to-brine/water ratio constant.

We investigated various container types and materials to determine which containers and lids minimize the loss of water and salt. In this experiment we placed DI water or WIPP brines in various bottles, then periodically measured the weight loss and brine conductivity. Bottles were put into a 70 °C oven to promote the water and salt loss. Among all the tested bottles the Wheaton glass serum bottle, Wheaton high density polyethylene (HDPE) serum bottle and Nalgene HDPE centrifuge bottle had the least weight loss. The weight loss was found to be independent of the volume of water originally emplaced in the bottle. In 22 days, the Wheaton glass serum bottle filled with 100 ml of brine lost 3.6 g (WIPP-MM MgO-1, p 96). The Wheaton HDPE serum bottle filled with 100 ml of DI water and HDPE centrifuge bottle filled with 1 ml or 10 ml of DI water lost 0.47 g and 0.51 g in 19 days, respectively (see WIPP-MM MgO-2, p 71). As long as brine remained in the bottles, no salt creep was observed.

5.2 Tracer Dyes

In some of the accelerated hydration samples we added a small amount of tracer dye, methylene blue or KI, into DI water to characterize hydration-reaction-front morphology at various times using image analysis. The KI has not worked well thus far as a tracer dye. Upon placing the methylene blue and Mesh 10 (~ 2 mm) particles of MM MgO together at 70 °C in DI water, the dye was able to completely penetrate Mesh 10 (~ 2 mm) particles within 1 hour, as shown in Figure 7.

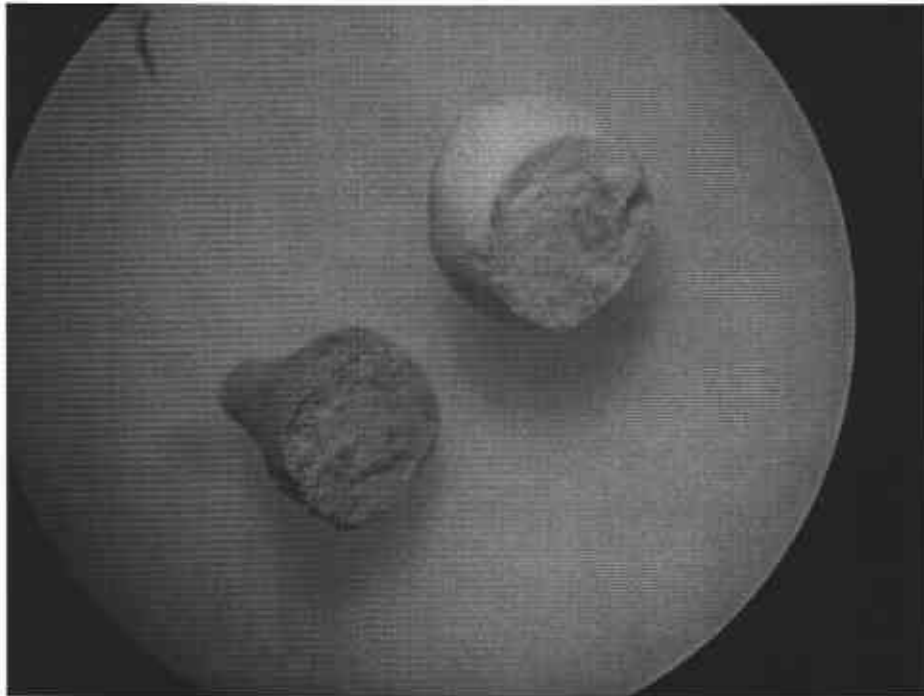


Figure 7. Image of a sliced dry Mesh 10 (~ 2 mm) MM MgO particle (upper right) compared to a sliced Mesh 10 (~ 2 mm) MM MgO (lower left) particle after being inundated in DI water containing methylene blue dye at 70 °C for 1 hour. Notice that the dye has completely penetrated the particle. This image is documented in scientific notebook WIPP-MM MgO-7, beginning on p 63.

Given the rapid time scale over which the dye penetrated the MgO particle (< 1 hour) compared to the time required for full hydration (43 days, see Subsection 5.4) one would conclude that diffusion does not control the MgO hydration rate since the diffusion constant increases only modestly with temperature ($D \sim \sqrt{T}$, in which D is the diffusion coefficient and T is absolute temperature). As will be shown below in Subsection 5.7.2, this conclusion appears to be true for the hydration of the larger particles, but diffusion may play a role in the kinetics of the finer particles.

5.3 Experiment Matrix

A fractional-factorial experimental matrix (Box et al., 1978) was designed using the Minitab statistical software package; Table 10 describes the experimental matrix. Wheaton HDPE serum bottles (125 ml) or Nalgene HDPE centrifuge tubes (30 ml) containing DI water and MM MgO were placed either in a VWR oven or in a New Brunswick Scientific water-bath shaker set to a shaking speed of 150 rpm. Both the oven and water-bath shaker were set to 70 °C. In order to accurately measure the MgO hydration rate, we did LOI and carbon coulometer tests on as-received MM MgO to determine if any MgO had been hydrated or carbonated before the hydration experiments were begun. Five bottles of MgO were randomly selected for the LOI test. The average brucite mole % in as-received MM MgO was found to be $0.19\% \pm 0.047\%$ (one sigma, see the Excel spreadsheet MgO packed in bottles LOI.xls). The carbon wt % of four bottles of MgO was tested by a UIC Inc CO₂ coulometer model CM504 with furnace apparatus model CM5120. The average carbon wt % was found to be 0.006 ± 0.002 (one sigma, see the Excel spreadsheet MgO packed in bottles LOI.xls).

The two MgO particle sizes with the highest particle size fraction were used in the accelerated inundated hydration experiments. The larger particle size used were those particles between 1.0-2.0 mm (between mesh 10 and 18, see Table 3) which accounted for 32 wt % of the as-received MM MgO. The smaller particle size used were those particles less than 75 µm (less than mesh 200) and accounted for 18 wt % of the as-received MM MgO.

Three WIPP-relevant MgO-to-liquid ratios (1 g/ml, 0.4 g/ml, and 0.05 g/ml) were used in the accelerated, inundated hydration experiments. Nemer (2006b) has shown that a range of 0.001 to 10 g/ml brackets the expected range of MgO-to-brine ratios in the WIPP. Previous work with Premier MgO was conducted with a MgO-to-liquid ratio equal to 0.05 g/ml. Therefore including the 0.05 g/ml ratio in our experiments enabled us to compare results to those of Premier. It will be shown below (see Subsection 5.4) that the MgO-to-liquid ratio was not a significant factor in the accelerated inundated hydration experiments.

Table 10. Accelerated, Inundated Hydration Experimental Matrix.

Experiment	ID ⁴	Motion ¹	Particle Size ²	MgO/water Ratio ³
1	Ahy-m-sml-tu	1	1	1
2	Ahy-m(8gmgo)-sml-tu	1	1	2
3	Ahy-m-sml-bo	1	1	3
4	Ahy-m-big-tu	1	2	1
5	Ahy-m(8gmgo)-big-tu	1	2	2
6	Ahy-m-big-bo	1	2	3
7	Ahy-s-sml-tu	2	1	1
8	Ahy-s(8gmgo)-sml-tu	2	1	2
9	Ahy-s-sml-bo	2	1	3
10	Ahy-s-big-tu	2	2	1
11	Ahy-s(8gmgo)-big-tu	2	2	2
12	Ahy-s-big-bo	2	2	3

1. Samples with Motion level 1 were placed inside oven. Samples with Motion level 2 were shaken at 150rpm in a water-bath shaker.
2. Particle size level 1 represents MgO with particle size between 1.0 mm - 2.0 mm. Particle size level 2 represents MgO with particle size less than 75 μ m.
3. Samples with MgO/water ratio level 1 contained 10 g of MM MgO and 10 ml of DI water. Samples with MgO/water ratio level 2 contained 8 g of MM MgO and 20 ml of DI water. Samples with MgO/water ratio level 3 contained 5 g of MM MgO and 100ml of DI water.
4. In the sample ID, Ahy means accelerated hydration. S means samples were kept in water bath shaker while M means samples were kept in oven without any motion. Big indicates the larger particle size while sml indicates the smaller particle size. Tu indicates that a centrifuge tube was used containing 10g of MM MgO and 10ml of DI water; (8g MgO) represents experiments with 8g of MM MgO and 20ml DI water kept in a centrifuge tube.

Bo represents experiments with the lowest MgO/water ratio (5g MgO and 100ml of DI water) in plastic serum bottles.

Information Only

5.4 Factors Influencing the Hydration Rate

Experiments were performed on MM MgO in DI water at 70 °C for 43 days. Duplicate samples were prepared for each experiment. The solid portion of the hydrated sample was filtered out using Whatman #40 filter paper and then dried in the lab air. An LOI test was then performed on the dried sample, from which the brucite mol % was calculated. To avoid further need for the assumptions made in Subsection 4 on how the mole percent of brucite in hydrated MM MgO is calculated, from this point forward we use the fraction of periclase converted to brucite,

$$W = \frac{X_{brucite}(t)}{X_{periclase}}, \quad (17)$$

as our measure of the reaction progress. Here $X_{brucite}(t)$ is the mol fraction of brucite in the hydrated sample at time t , and $X_{periclase}$ is the initial mole fraction of periclase as described above in Subsection 4. Notice that W varies from 0 to ~ 1, and is independent of the assumptions made in Subsection 4 to calculate $X_{periclase}$, since those same assumptions are also made to calculate $X_{brucite}(t)$. The results showed that the large-particle-size samples hydrated further than the small-particle-size samples in the experimental time period, and thus we used the average hydration of all the large-particle-size samples at 43 days as our measure of complete hydration $X_{brucite}(\infty) = X_{periclase}$. It is important to note that the average of the large-particle size samples was consistent with the results of Subsection 4. At the end of 43 days, the average W of the small-particle-size samples was $W = 0.9735$ and by our above definition the large-particle-size reached $W=1$. According to X-ray diffraction (XRD) patterns, brucite was the only product of MgO hydration in DI water. There were still small peaks of periclase in the hydration product of small-particle-MgO when samples were collected at 43 days (recorded in supplemental binder mmMgO-XRD-1). Given more time, we expect the small particle size MgO would completely hydrate.

Figure 8-11 show the mole percent of brucite in the hydrated samples versus time for the different factors and levels listed in Table 10. Looking at Figure 8 and Figure 10 one can see that the small-particle-size samples hydrated faster than the large particle size during the first few days, which is probably due to the larger specific surface area (m^2/g) of the smaller particles. However for the remainder of the experiment, the large-particle-size samples hydrated faster than the small particle size. There are no obvious differences between experiments that were continuously stirred in a water bath shaker and those that were kept in the oven. The MgO-water ratio did not significantly influence the hydration rate either. These visual observations have been confirmed by the Minitab analysis, as discussed below.

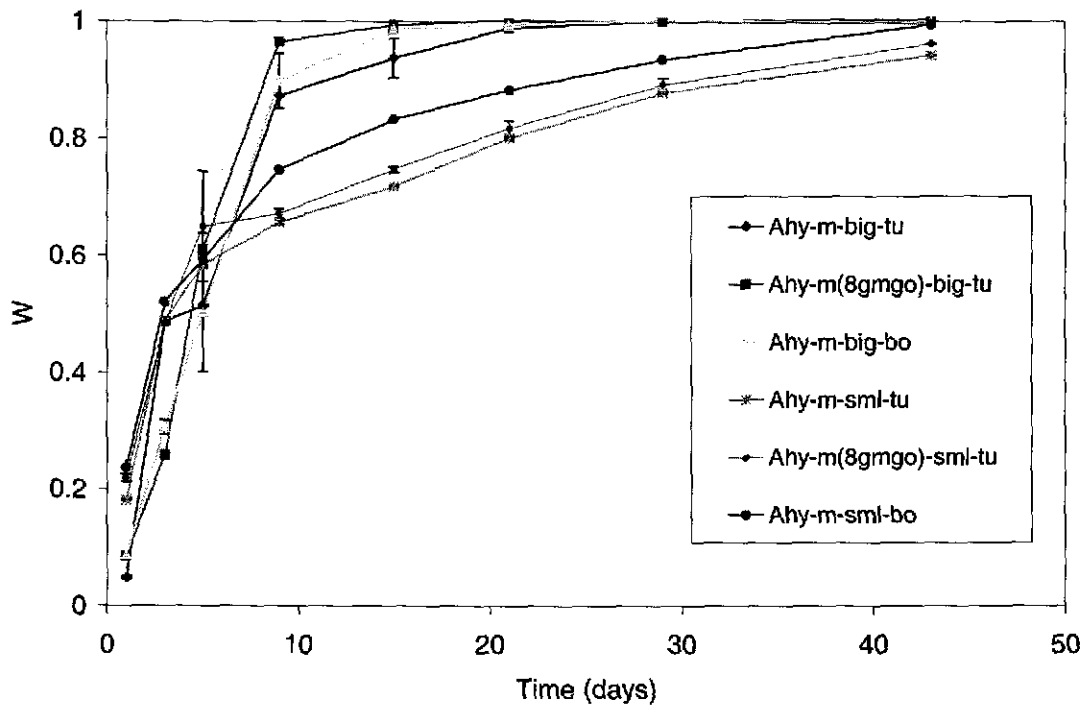


Figure 8. MM MgO hydration progress (W) versus time (days) for experiments carried out in DI water at 70 °C in an oven (not shaken). The conditions for each sample identified in the legend can be found in Table 10.

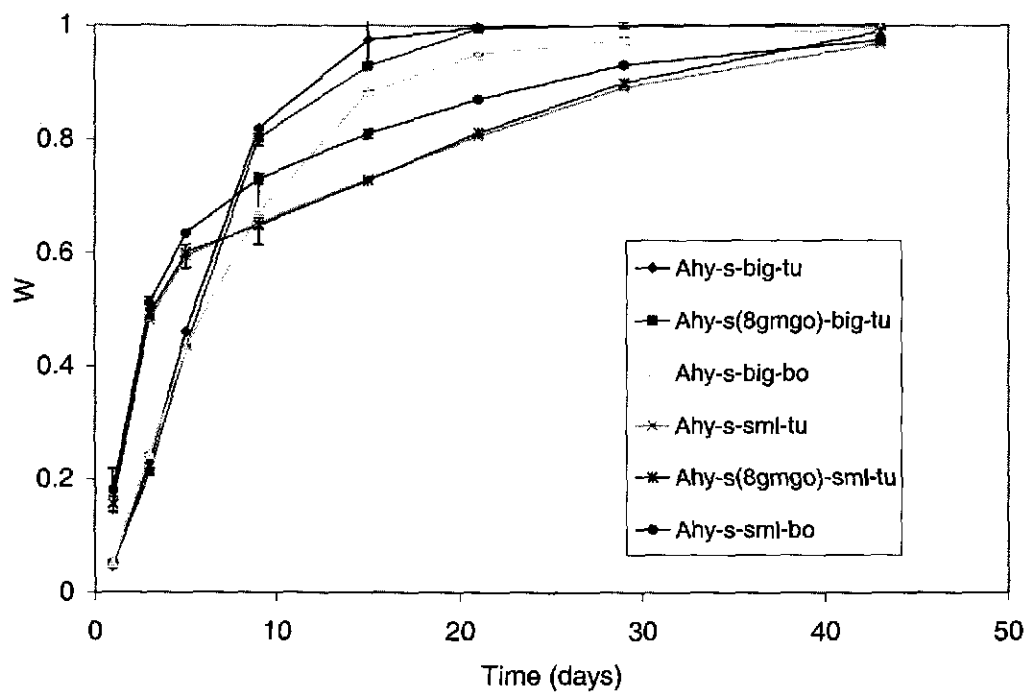


Figure 9. Same as Figure 8 for experiments carried out in water bath shaker at 70 °C at a shaking speed of 150 rpm.

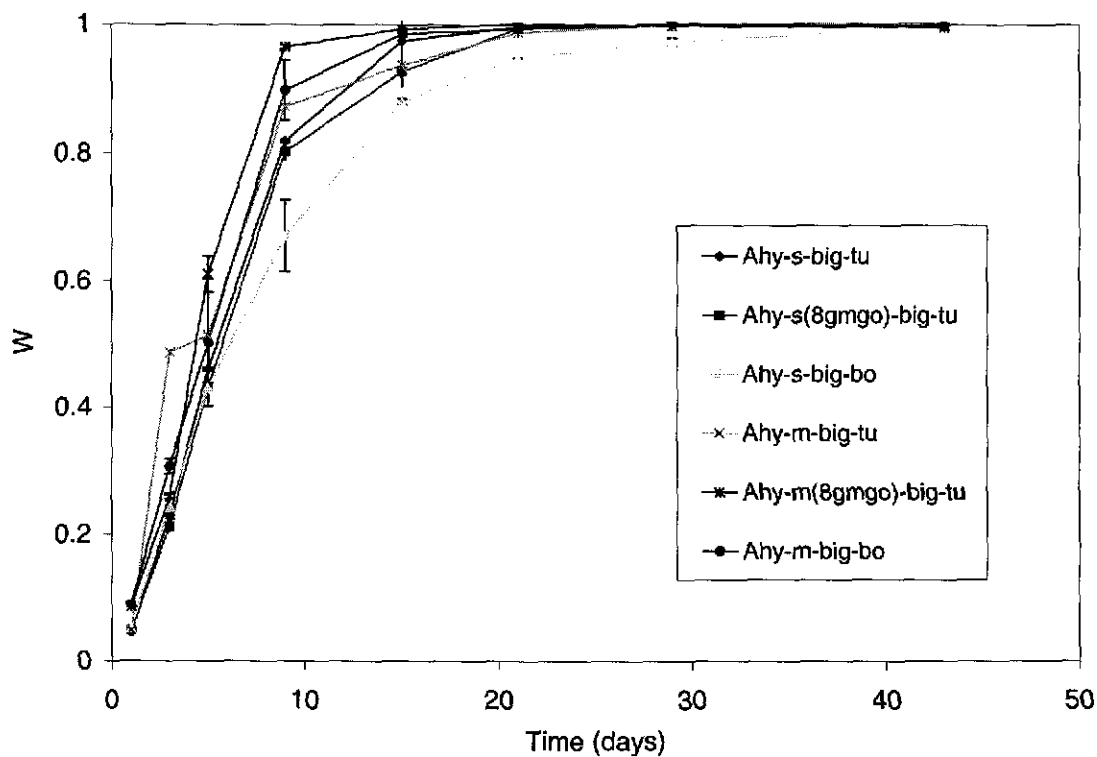


Figure 10. MM MgO hydration progress (W) versus time (days) for experiments carried out in DI water at 70 °C with big particles.

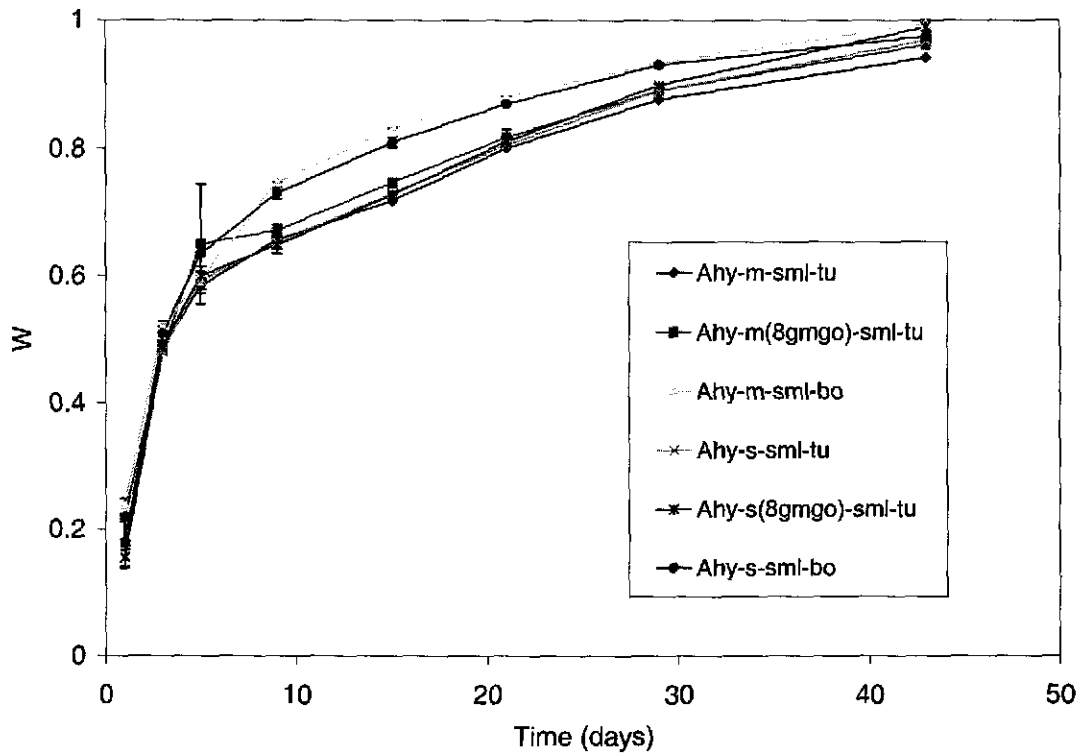


Figure 11. Same as Figure 10 for experiments carried out in water bath shaker at 70 °C at a shaking speed of 150 rpm, with small particles.

Minitab fits a linear model to the response (W) as a function of the effect variables (motion, particle size, and MgO/water ratio) at each time by multiple linear regression,

$$W(t) = C_{Mg(OH)_2}(t) + C_{mot}(t)Y_{mot} + C_{ps}(t)Y_{ps} + C_{Mwr}(t)Y_{Mwr} \quad (18)$$

where the terms $C(t)$ are the coefficients of the fit for the three factors (C_{mot} , C_{ps} , C_{Mwr}) and the intercept $C_{Mg(OH)_2}$; the values of the coefficients are given below in Table 11. Here mot stands for motion, ps stands for particle size, and Mwr stands for MgO/water ratio. The Y terms are the indicator values given in the right hand columns of Table 10. For example, if we wished to calculate the expected value for $W(t)$ on day 1, given no motion (samples kept in oven) $Y_{mot} = 1$, the larger particle size $Y_{ps} = 1$, and the smallest MgO/water ratio $Y_{Mwr} = 3$, using Equation 18 and the coefficients listed in Table 11 we find

$$W(t) = 0.3359 + (-0.03384)(1) + (-0.1271)(1) + (0.01591)(3) = 0.2227, \quad (19)$$

which is close to the value of 0.2174 actually obtained.

While Equation 18 can be used to calculate expected values and an uncertainty in that value, the purpose of this designed experiment was to determine which factors are most

important in determining the hydration rate. To do this one looks at the magnitude of the coefficients $C(t)$ and the P values for each coefficient. Note that because the independent variables (motion, particle size, MgO-water ratio) are in “coded” variables all of the coefficients $C(t)$ have approximately the same scale, that is if they were equally important they would have approximately equal magnitude. Table 11 lists the P value for each of the three factors at each time. The lower the P value, the higher the probability that a factor is significant. As a rule of thumb, a factor is considered significant if the P value is 0.10 or less. Table 11 also lists the R^2 value at each time, which indicates the fraction of the total variation in $Y_{Mg(OH)_2}(t)$ that is accounted for by Equation 18. Thus on day one 94.8 % of the population of values is covered by Equation 18.

Examining Table 11, we can see that as hydration proceeds motion becomes less important (P value increasing), but particle size is always a critical factor (P value consistently small). We can also see that MgO/water ratio becomes increasingly important as hydration proceeds (decreasing P value, but C_{Mwr} still small compared to C_{ps}). This can be explained by the observations on samples with the highest MgO/water ratio, 10 g MgO in 10 ml DI water. As the hydration proceeded less and less water was available. By the seventh day, the larger particle size samples had no visible water left, and at day 15 there was not enough water to check pH for the smaller particle size samples.

Table 11. Minitab Report on Hydration Rate and Reaction Factors.

Time (days)	$C_{Mg(OH)2}$ (intercept)	C_{mot} (motion)	P	C_{ps} (particle size)	P	C_{Mwr} (MgO/Water ratio)	P	R^2
1	0.3359	-0.03384	0	-0.1271	0.000	0.01591	0.001	0.948
3	0.8231	-0.06378	0.023	-0.2059	0.000	-0.008524	0.419	0.779
5	0.7993	-0.05051	0.33	-0.1171	0.000	0.001119	0.934	0.626
9	0.6379	-0.07985	0.01	0.1554	0.000	0.004334	0.797	0.68
15	0.5672	-0.02313	0.205	0.1933	0.000	0.01554	0.171	0.87
21	0.6575	-0.006213	0.562	0.1593	0.000	0.01042	0.127	0.926
29	0.7920	0.0009551	0.891	0.09419	0.000	0.007249	0.105	0.911
43	0.9218	0.002958	0.572	0.03056	0.000	0.006595	0.053	0.67

5.5 Volume Change upon Hydration

An interesting phenomenon that was observed was that the larger-particle-size samples expanded in the longitudinal direction of the centrifuge tubes while the small-particle-size samples expanded in the radial direction of the centrifuge tubes (see lower image in Figure 12). We did not observe a bulge in serum bottles. The centrifuge tube wall is 2 mm thick. Thus expanding the centrifuge tube radially requires considerable force. Given this confining pressure, one might expect that the small particles packed much tighter (in centrifuge tubes) than the large-particle samples. Based on this hypothesis, we might expect that the tightly packed samples would have smaller porosity. This might explain why (1) the larger particles hydrated faster than smaller particles; (2) small-particle samples packed in serum bottles hydrated faster than small-particle samples packed in centrifuge tubes; (3) large-particle-size samples in serum bottles did not hydrate faster than large-particle-size samples in centrifuge tubes. This phenomenon may also indicate that the small-particle samples were not well stirred in the shaker bath. Once the reaction started the small-particle samples become caked in the vials. Thus the shaker was probably ineffective at this point on the small-particle samples, which is consistent with the Minitab report in Section 5.4.

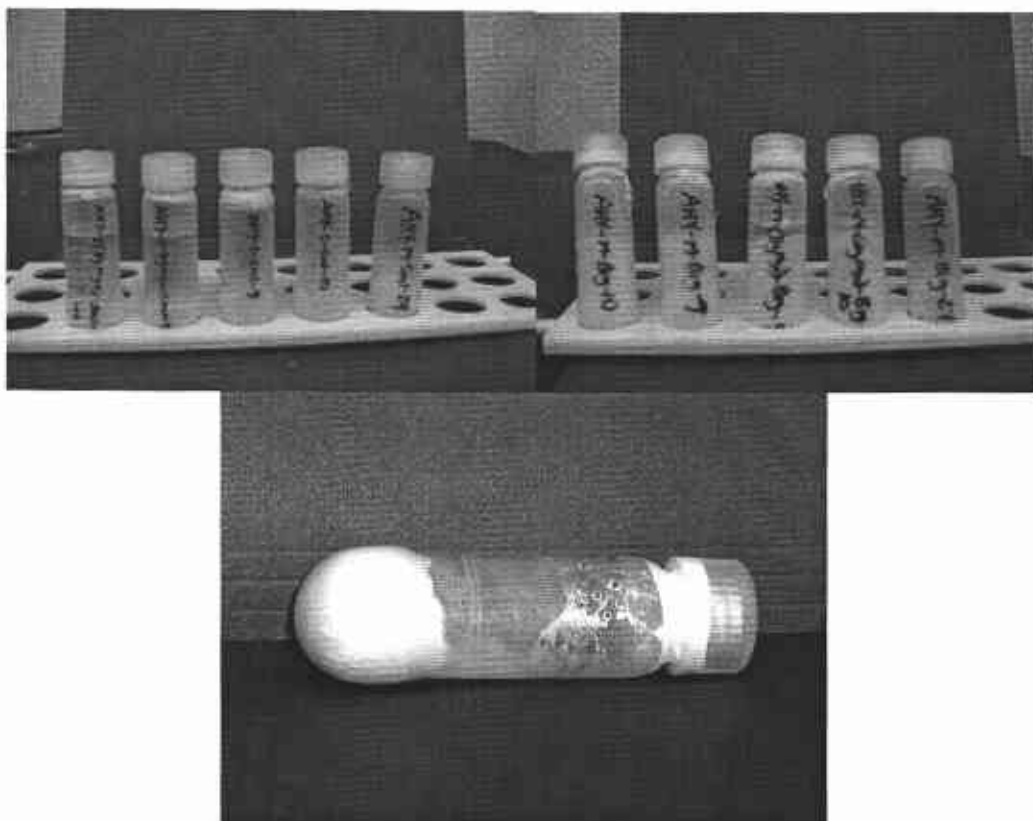


Figure 12. Digital pictures of MM MgO accelerated hydration in DI water at 70 °C. The pictures were taken on the ninth day of hydration. For scale, in the top two pictures the 5th centrifuge tube from the right shows 10 g of dry MgO in a centrifuge tube with the same particle size as the rest of the row of bottles (small particle size in the top left image, large particle size in the top right image). The bottom picture highlights the expanded radius of the bottom of the centrifuge tube.

5.6 Hydration Mechanisms

In dilute solutions, researchers have found that MgO hydration proceeds by dissolution of the MgO followed by precipitation of brucite crystals, usually attached to the MgO surface (Fruhirth et al., 1985; Filippou et al., 1999). We have taken SEM images of hydrated MM MgO at different times to examine this process. Figure 13 - Figure 16 show the hydration of small-particle-size samples before hydration, after 1 day, after 9 days, and after 43 days respectively, in DI water at 70 °C. Figure 17 - Figure 20 are a higher magnification version of Figure 13 - Figure 16. The figures indicate that hydration proceeds by dissolving periclase and reprecipitating it as fine hexagonal brucite crystals on the outside of the periclase particles. The small hexagonal crystals in Figure 21 illustrate hydration of MM MgO after 26 days in DI water at 70 °C. By the end of 43 days, the periclase particles have completely reorganized into clumpy plate-like particles with much smaller crystals.

It is unclear from Figure 13 - Figure 20 whether porosity is decreasing as a result of hydration, however, as shown in Subsection 5.7.2, diffusion may be important for hydration kinetics of the smaller particles. Rocha (2004) concluded that at high temperature, the hydration of MgO is at first governed by MgO dissolution (surface-area control), then as the reaction progresses, both the surface and pores of MgO are covered by Mg(OH)₂, changing the porosity of the solid. As a result, the diffusion is hindered inside particles (diffusive control). Rocha (2004) observed that the kinetics of MgO hydration changed from surface-area control to diffusive control at $W > 0.6$.

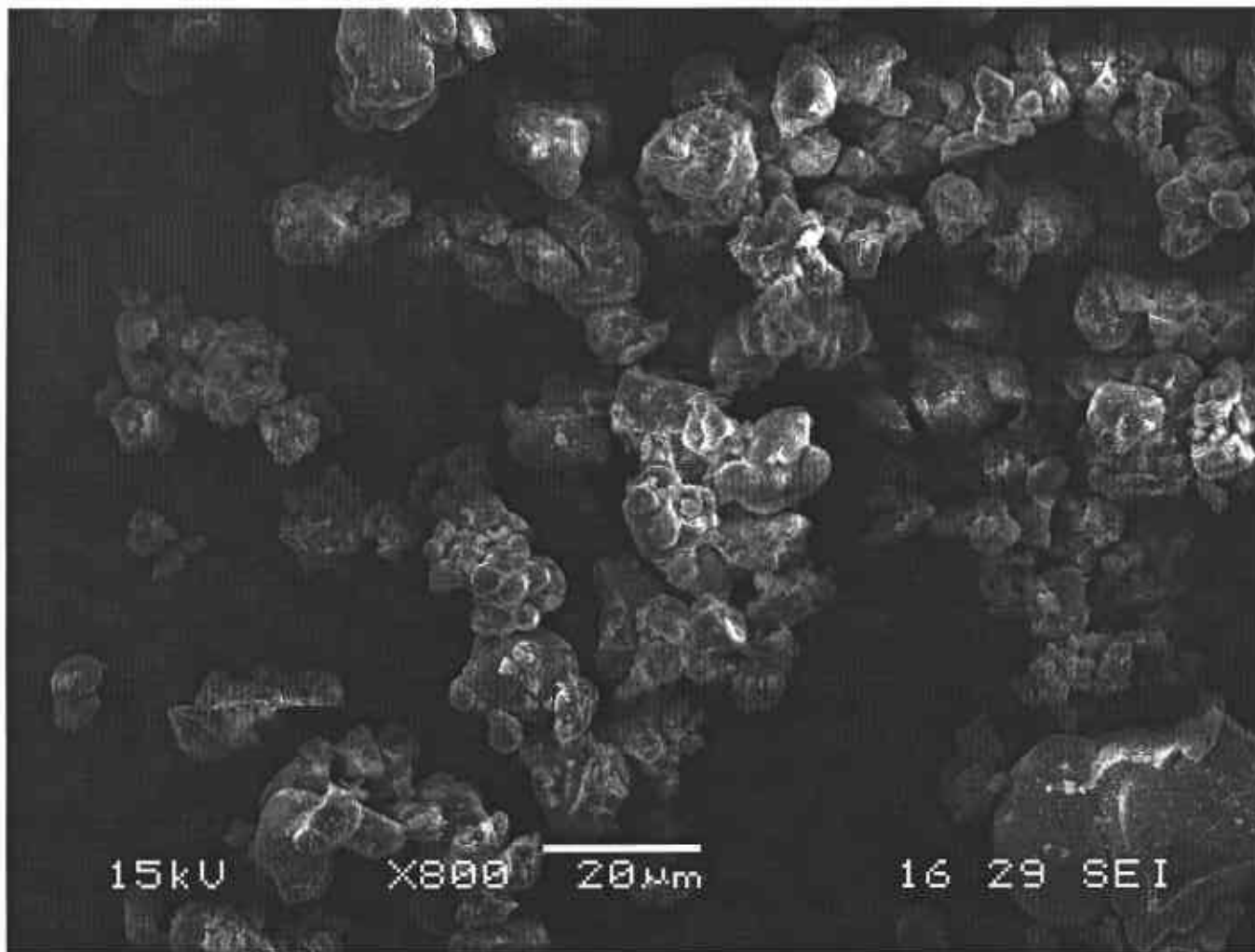


Figure 13. Image of small-particle size sample before hydration. This image is h1i1b.bmp in SN WIPP-MM MgO-7 on p 72.

Information Only

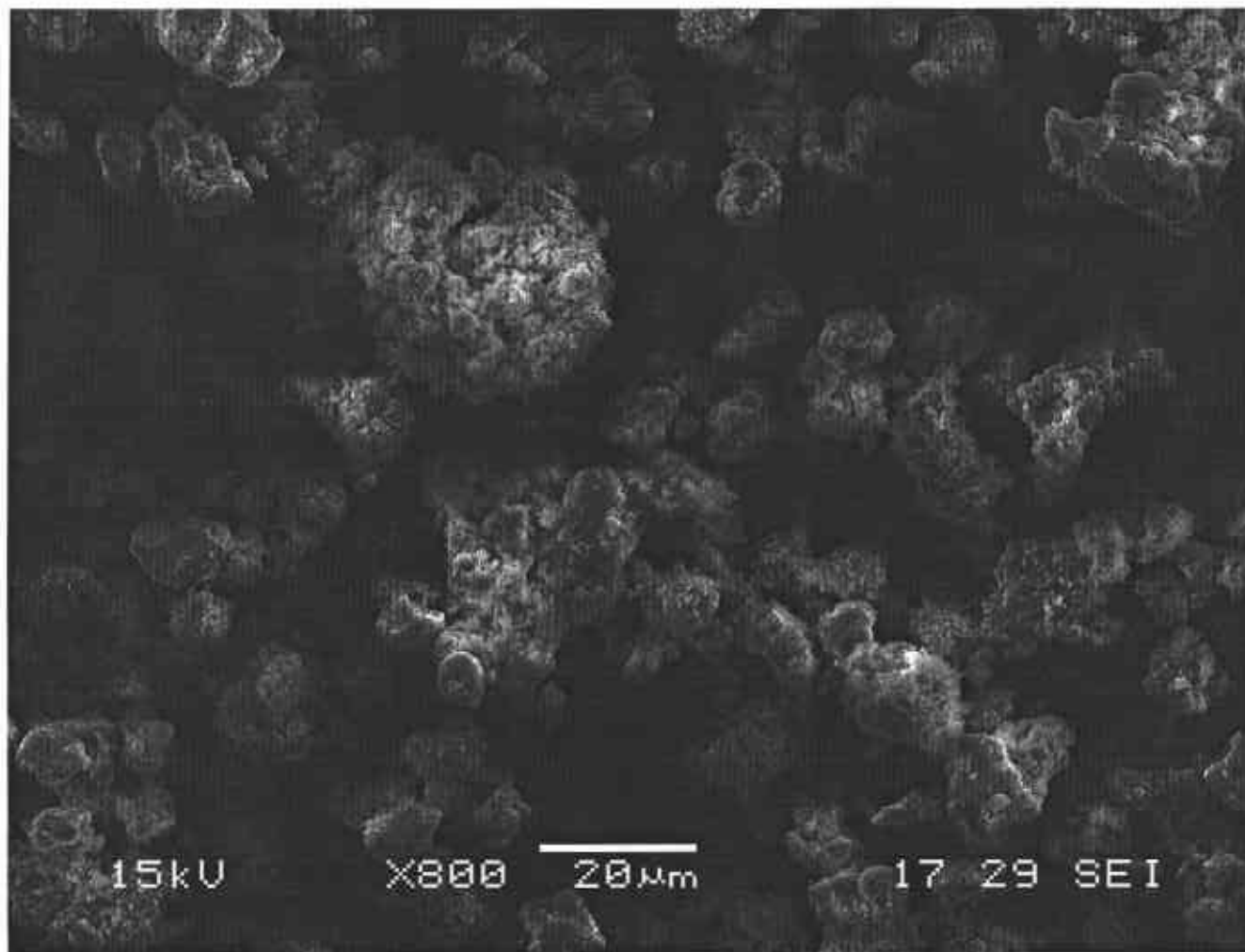


Figure 14. Image of small-particle-size sample after 1 day hydration at 70 °C in DI water in the oven. This image is h2i1b.bmp in SN WIPP-MM MgO-7 on p 72.

Information Only

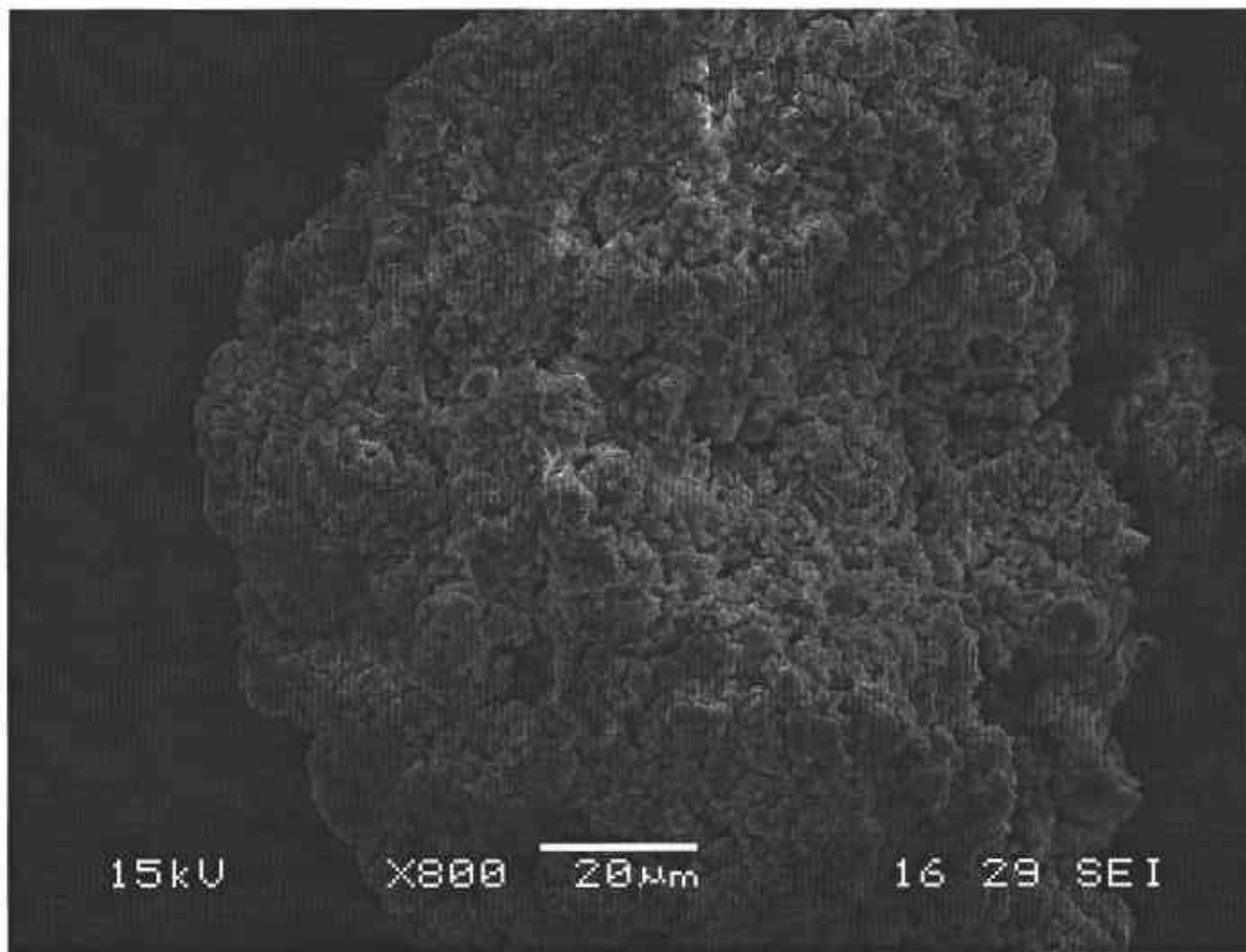


Figure 15. Image of small-particle-size sample after 9 days of hydration at 70 °C in DI water. This image is h3i1b.bmp in SN WIPP-MM MgO-7 on p 72.

Information Only

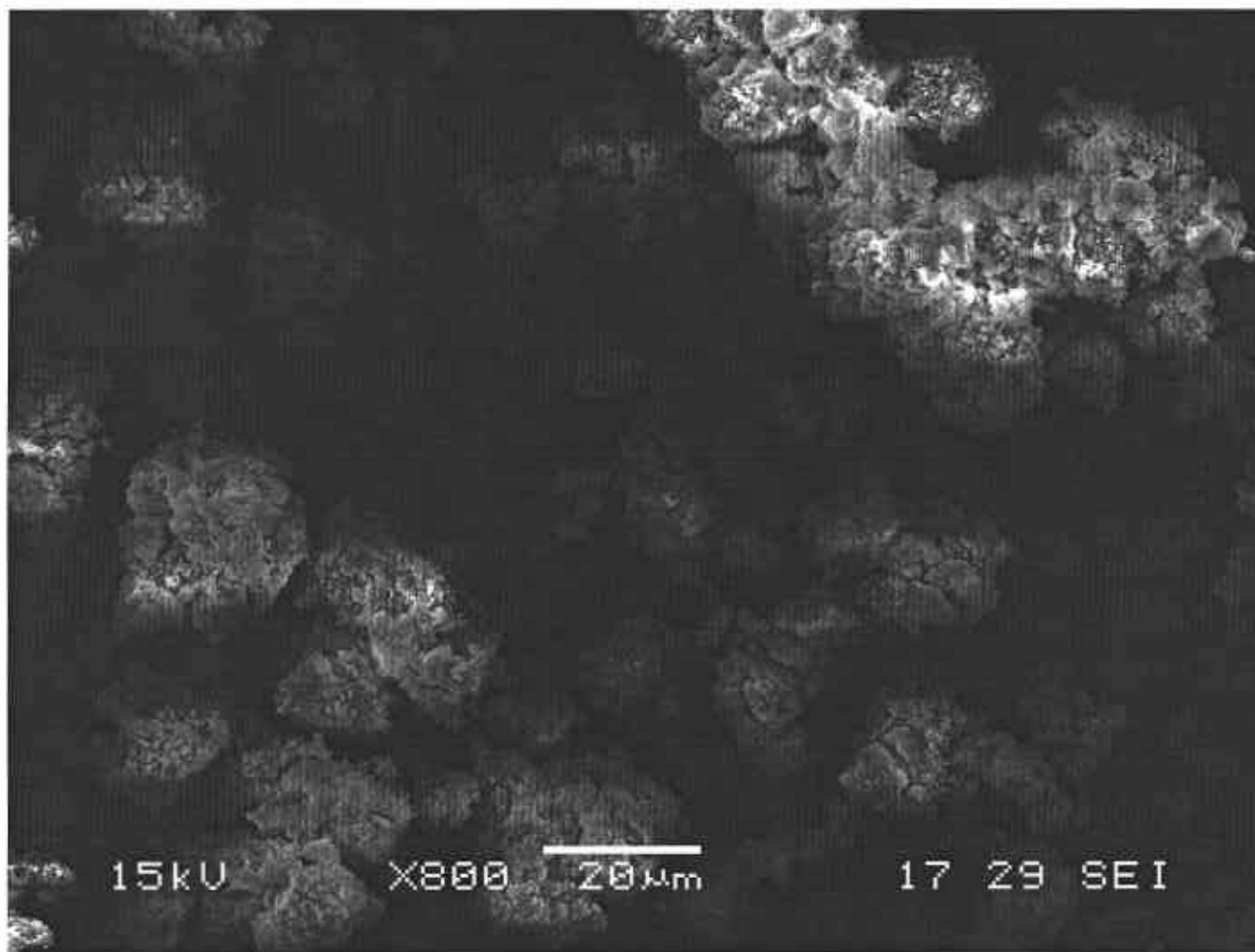


Figure 16. Image of small-particle-size sample after 43 days of hydration at 70 °C in DI water. This image is h6i1b.bmp in SN WIPP-MM MgO-7 on p 72.

Information Only

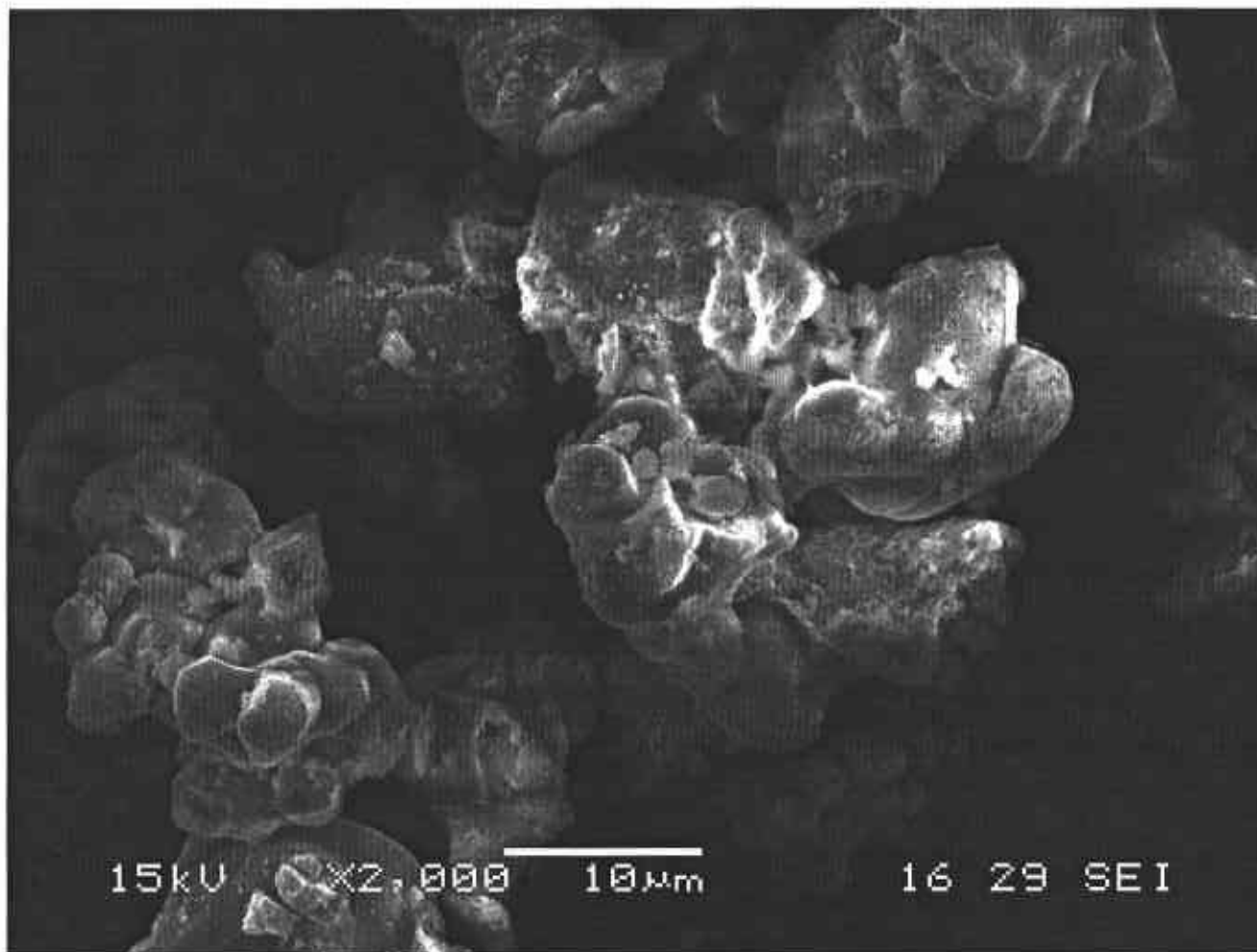


Figure 17. Same as Figure 13 at higher magnification. This image is h11c.bmp in SN WIPP-MM MgO-7 on p 72.

Information Only



Figure 18. Same as Figure 14 at higher magnification. This image is h2i1c.bmp in SN WIPP-MM MgO-7 on p 72.

Information Only

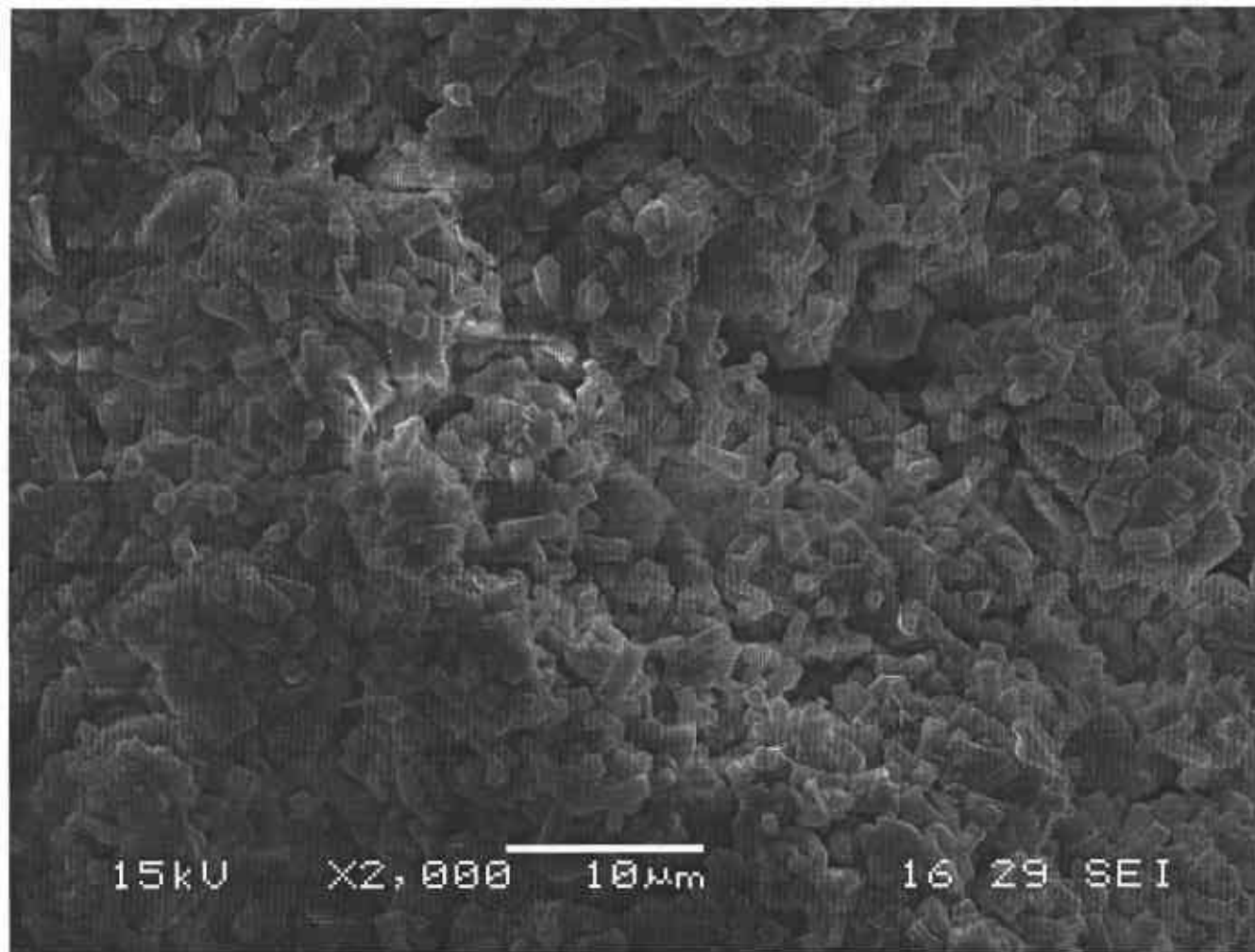


Figure 19. Same as Figure 15 at higher magnification. This image is h3i1c.bmp in SN WIPP-MM MgO-7 on p 72.

Information Only

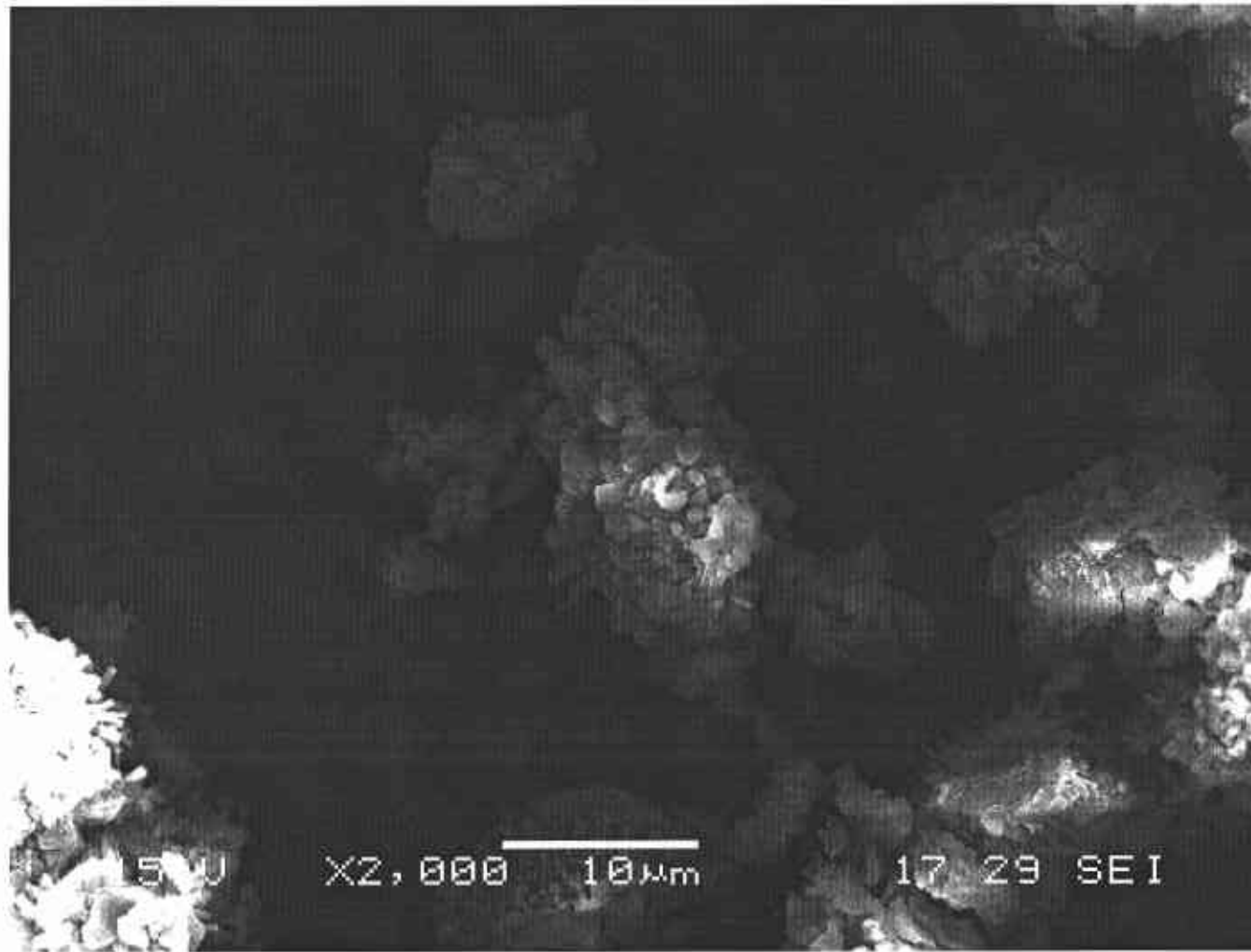


Figure 20. Same as Figure 16 at higher magnification. This image is h611c.bmp in SN WIPP-MM MgO-7 on p 72.

Information Only

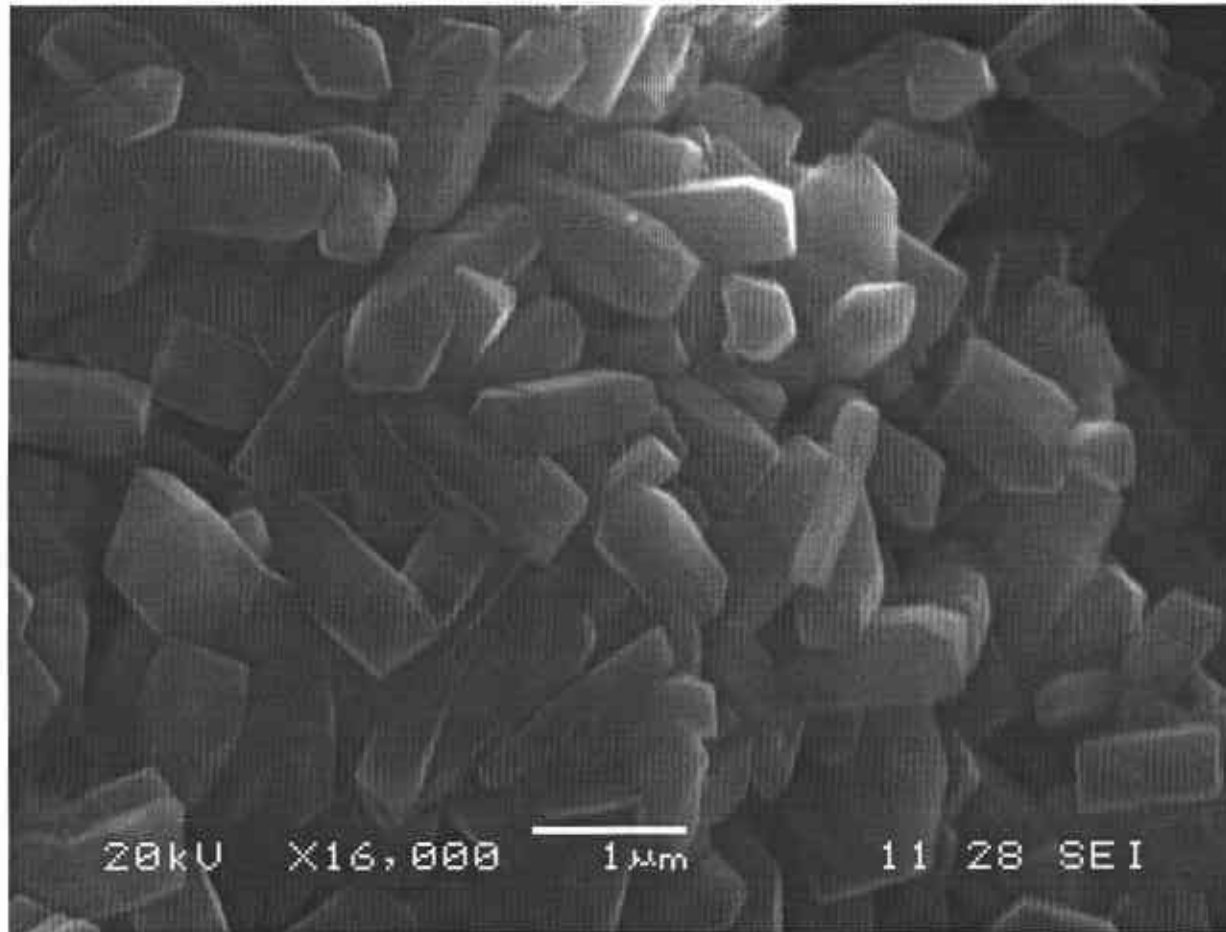


Figure 21. Hexagonal crystals formed after 26 day of hydration of MM MgO. This image is 104h4i4c.bmp and can be found in SN WIPP-MM MgO-4, p 16.

Information Only

5.7 Comparison with Theoretical Models

In this Subsection we fit the accelerated-inundated hydration data to four different kinetic models. Among the four models, one model is surface-area controlled, the other three are diffusion-controlled. As will be shown, the large-particle-size hydration data are consistent with the surface-area controlled model, and the small-particle-size hydration data are consistent with diffusion control.

5.7.1 Background on Models

The surface-area controlled model assumes that the hydration kinetics are controlled by the number of active sites on the reacting surface of a sphere that is shrinking as the reaction proceeds (Layden and Brindley, 1963). According to this model there is a linear relation between $y = 1 - (1 - W)^{1/3}$ and time,

$$y_1 = 1 - (1 - W)^{1/3} = k_1 t. \quad (20)$$

Here k_1 is the reaction-rate constant with dimensions of time^{-1} , t is time.

For kinetics that is controlled by diffusion through the brucite layer to the periclase reaction interface, there are several models to choose from. Jander developed a model which assumes that the interface is planar (Jander, 1927),

$$y_2 = [1 - (1 - W)^{1/3}]^2 = k_2 t, \quad (21)$$

where k_2 is the reaction-rate constant. Carter developed a model similar to that of Jander except they assume a spherical interface (Carter, 1961),

$$y_3 = \frac{[1 + (z - 1)W]^{2/3} + (z - 1)(1 - W)^{2/3} - z}{2(1 - z)} = k_3 t. \quad (22)$$

Here z is the ratio of the molar volume of the product to the molar volume of the reactant (which we take to be brucite and periclase respectively), and k_3 is the reaction-rate constant. If we assume no volume change occurs during the reaction (i.e. compaction), then $Z = 1$, and we obtain Ginstilin's model (Ginstling and Brounshtein, 1950),

$$y_4 = 1 - 2/3W - (1 - W)^{2/3} = k_4 t. \quad (23)$$

where k_4 is the reaction-rate constant.

5.7.2 Modeling Results

The data (W versus t) were fitted to the four models listed above (y_1, \dots, y_4) to obtain the respective reaction-rate constants, and to determine if a particular model or class of models fit the data better than another. This information may guide us as to what models are appropriate for the long-term hydration studies, which may not reach complete hydration over experimental time scales. The resulting R^2 values are shown below in Table 12. This was calculated in the Microsoft Excel Spreadsheet AHY(hydration rate) mbn version 2.xls (datasheet hydration rate-different (6)) using the Excel Function LINEST, which also contains the k_i , if the reader desires this information. It is clear from the R^2 values in Table 12 that diffusion (models 2 through 4) may be important for the small particles. Whether diffusion is controlled by a rind around individual small particles or by transport through a cake of small partially hydrated particles is unclear. For the large particles, surface-area control (model 1) had the largest R^2 .

Table 12. R^2 Values for Linear Regression of MM MgO Hydration in DI Water at 70 °C with the Four Models Described in Subsection 5.7.1.

Sample ID	Model 1	Model 2	Model 3	Model 4
Ahy-m-big-bo	0.97	0.96	0.96	0.96
Ahy-m-big-tu	0.98	0.97	0.98	0.98
Ahy-s-big-bo	0.96	0.99	0.96	0.97
Ahy-s-big-tu	0.99	0.95	0.98	0.97
Ahy-m(8gmgo)-big-tu	0.97	0.94	0.95	0.94
Ahy-s(8gmgo)-big-tu	0.99	0.92	0.98	0.97
Average of large particle samples	0.98	0.95	0.97	0.96
Ahy-m-sml-bo	0.94	0.97	0.97	0.99
Ahy-m-sml-tu	0.91	1.00	0.97	0.98
Ahy-s-sml-bo	0.91	1.00	0.95	0.97
Ahy-s-sml-tu	0.93	0.99	0.98	0.99
Ahy-m(8gmgo)-sml-tu	0.91	0.99	0.96	0.98
ahy-s(8gmgo)-sml-tu	0.94	0.95	0.98	0.99
Average of Small Particle Samples	0.92	0.98	0.97	0.98

6 CONCLUSIONS

Two major tasks in the test plan of Deng et al. (2006) have thus far been completed: characterization of MM MgO and the accelerated inundated hydration study. Characterization showed that the mole % of periclase in MM MgO is $96 \% \pm 2 \%$. The mole % calculation included a number of conservative assumptions which lower the calculated result.

The purpose of the accelerated inundated hydration study was to look at the reaction mechanisms of Martin Marietta MgO hydration to be better able to design and interpret the results of long-term hydration and carbonation studies of the same material. As a result of this study we have determined that different mechanisms may be important for different particle sizes, surface-control for larger particles and diffusion for small particles. Long-term hydration and carbonation studies are currently under way and will be reported on in the next milestone report.

7 REFERENCES

- Alarcon-Ruiz, L., G. Platret, E. Massieu and A. Ehrlacher. 2005. "The Use of Thermal Analysis in Assessing the Effect of Temperature on a Cement Paste," *Cement and Concrete Research*. Vol. 35, 609-613.
- Bates, R.L., and J.A. Jackson, Eds. 1984. *Dictionary of Geological Terms*, Third Edition. New York, NY: Anchor Books (Doubleday).
- Box, G.E.P., W.G. Hunter and J.S. Hunter. 1978. *Statistics for Experimenters; An Introduction to Design, Data Analysis, and Model Building*. New York: John Wiley & Sons.
- Bynum, R.V. 1997. "Confirmation of the Ability of a Designed Backfill to Control the Chemical Environment in the WIPP." TP 97-01, Rev. 1, April 15, 1997. Albuquerque, NM: Sandia National Laboratories. ERMS 419286.
- Bynum, R.V., C.T. Stockman, H.W. Papenguth, Y. Wang, A.C. Peterson, J.L. Krumhansl, E.J. Nowak, J. Cotton, S.J. Patchet, and M.S.Y. Chu. 1998. "Identification and Evaluation of Appropriate Backfills for the Waste Isolation Pilot Plant (WIPP)," *International Workshop on the Uses of Backfill in Nuclear Waste Repositories, Carlsbad, New Mexico, US, May 1998*. Eds. D.G Bennett, H.W. Papenguth, M.S.Y. Chu, D.A. Galson, S.L. Duerden, and M.L. Matthews. Bristol, United Kingdom: Environment Agency. R&D Technical Report pp 178, 2-178 to 2-187. ERMS 250807, SAND98-1026C.
- Carter, R.E. 1961. "Kinetic Model for Solid-State Reactions," *The Journal of Chemical Physics*. Vol. 34, 2010-2015.
- Deer, W.A., R.A. Howie and J. Zussman. 1992. *An Introduction to The Rock Forming Minerals*. 2nd Edition. Essex, UK: Longman Group.
- Deng, H., M.B. Nemer, and Y. Xiong. 2006. "Experimental Study of MgO Reaction Pathways and Kinetics, Rev. 0." TP 06-03, Rev. 0, June 6, 2006. Carlsbad, NM: Sandia National Laboratories. ERMS 543633.
- Deng, H. 2006. "Use and Maintenance of the UIC Inc. Model CM5014 CO₂ Coulometer, CM 5130 Acidification Module and CM 5120 Furnace Apparatus." SNL WIPP Activity Project Specific Procedure SP 12-2, Rev. 1, March 13, 2006. Carlsbad, NM: Sandia National Laboratories. ERMS 542674.
- Fernandez, A.I., J.M. Chimenos, M. Segarra, M.A. Fernandez and F. Espiell. 1999. "Kinetic Study of Carbonation of MgO Slurries," *Hydrometallurgy*. Vol. 53, 155-167.

- Filippou, D., N. Katiforis, N. Papassiopi and K. Adam. 1999. "On the Kinetics of Magnesia Hydration in Magnesium Acetate Solutions," *Journal of Chemical Technology and Biotechnology*. Vol. 74, 322-328.
- Fisher Chemical. 2005. "Certificate of Analysis for Fisher FCC/USP Magnesium Hydroxide, Cat M342, Lot 025425, and Fisher Chemical Specifications and Analytical Methods Sheet for Magnesium Hydroxide." Fairlawn, NJ: Fisher Chemical. ERMS 544636.
- Fruhwirth, O., G.W. Herzog, I. Hollerer and A. Rachetti. 1985. "Dissolution and Hydration Kinetics of MgO," *Surface Technology*. Vol. 24, 301-317.
- Ginstling, A.M. and B. Brounshtein. 1950. "On Diffusion Kinetics of Reactions In Spherical Particles," *Zhurnal Prikladnoi Khimii (Journal of Applied Chemistry, USSR)*. Vol. 23, 1249-1259.
- Jander, W. 1927. "Reactions in Solid States at Room Temperature; I. Announcement the Rate of Reaction in Endothermic Conversions," *Zeitschrift für Anorganische und Allgemeine Chemie*. Vol. 163, 1-30.
- Kolthoff, I.M., P.J. Elving and E.B. Sandell. 1962. *Treatise on Analytical Chemistry, Part II Analytical Chemistry of the Elements, Section A Systematic Analytical Chemistry of the Elements*. Volume 2. New York, NY: John Wiley & Sons.
- Krumhansl, J.L. 1997. "Continued Laboratory Research Program Directed at Chemical and Mechanical Effects of MgO Backfill on WIPP Repository Behavior, Rev. 0." SNL WIPP Test Plan (TP) 98-05, December 16, 1997. Carlsbad, NM: Sandia National Laboratories. ERMS 421381.
- Layden, G. K. and G. W. Brindley. 1963. "Kinetics of Vapor-Phase Hydration of Magnesium Oxide," *Journal of The American Ceramic Society*. Vol. 46, 518-522.
- Martin Marietta Magnesia Specialties Inc. 2006a. "Analysis of Shipment for Magnesium, Plant Shipping No SL2980076." Manistee, MI: Martin Marietta Magnesia Specialties Inc. ERMS 543900.
- Martin Marietta Magnesia Specialties Inc. 2006b. "Specifications Sheet for MagChem 10." Manistee, MI: Martin Marietta Magnesia Specialties Inc. ERMS 544635.
- Moody, D.C. 2006. Untitled letter from D.C. Moody to E.A. Cotsworth requesting EPA approval of the DOE's request reduce the amount of excess MgO currently being emplaced in the WIPP, April 10, 2006. Carlsbad, NM: U.S. Department of Energy Carlsbad Field Office. ERMS 543262.
- Nemer, M.B. 2006a. "Design Document for BRAGFLO Version 6.00." Carlsbad, NM: Sandia National Laboratories. ERMS 545015.

- Nemer, M.B. 2006b. "Expected Brine Volumes, Cumulative Brine Inflow, and MgO-to-Brine Solid-to-Liquid Ratio from PABC BRAGFLO Results." Memo to the Records Center, March 3, 2006. Carlsbad, NM: Sandia National Laboratories. ERMS 542612.
- Nemer, M.B. 2006c. "Software Installation and Checkout for BRAGFLO Version 6.00." Carlsbad, NM: Sandia National Laboratories. ERMS 545019.
- Nemer, M. B. 2006d. "Scanning Electronic Microscope Imaging and Energy Dispersive Spectroscopy." SNL WIPP Activity Project Specific Procedure SP 12-17, May 10, 2006. Carlsbad, NM: Sandia National Laboratories. ERMS 543306.
- Papenguth, H.W., J.L. Krumhansl, R.V. Bynum, Y. Wang, J.W. Kelly, H.L. Anderson, and E.J. Nowak. 1998. "Status of Research on Magnesium Oxide Backfill," *International Workshop on the Uses of Backfill in Nuclear Waste Repositories, Carlsbad, New Mexico, US, May 1998*. Eds. D.G Bennett, H.W. Papenguth, M.S.Y. Chu, D.A. Galson, S.L. Duerden, and M.L. Matthews. Bristol, United Kingdom: Environment Agency. R&D Technical Report P178, 3-43-3-63. SAND98-2582C.
- Rocha, S.D., M.B. Mansur and V.S. Ciminelli. 2004. "Kinetics and Mechanistic Analysis of Caustic Magnesia Hydration," *Journal of Chemical Technology and Biotechnology*. Vol. 79, 816-821.
- Snider, A.C. 2002. "MgO Studies: Experimental Work Conducted at SNL/Carlsbad. Efficacy of Premier Chemicals MgO as an Engineered Barrier," "Sandia National Laboratories Technical Baseline Reports; WBS 1.3.5.3, Compliance Monitoring; WBS 1.3.5.4, Repository Investigations; Milestone RI110; January 31, 2002." Carlsbad, NM: Sandia National Laboratories. ERMS 520467. 3.1-1 to 3.1-18.
- Stein, J.S. 2004. "Analysis Package for Direct Brine Releases: Compliance Recertification Application Rev. 1." Analysis Package. Carlsbad, NM: Sandia National Laboratories. ERMS 532344.
- Taylor, J.R. 1982. *An Introduction to Error Analysis, The study of Uncertainties in Physical Measurements*. Mill Valley, CA: University Science Books.
- Wall, N.A. 2005. "Preliminary Results for the Evaluation of Potential New MgO." Analysis Report, January 27, 2005. Carlsbad, NM: Sandia National Laboratories. ERMS 538514.

APPENDIX A. CALCULATIONS IN THE 90-922 RESULTS SPREADSHEET

The spreadsheet 90-922 results4.xls is organized as follows. Cells A1-E8 contain the weight percent (in the hydrated sample) of water lost from TGA experiments on hydrated MM MgO. The scientific notebook and page number are given in columns C and D. Cells A13-F19 contain the weight percent (in the hydrated sample) of water lost from LOI experiments on hydrated MM MgO using a Fisher programmable furnace. A run of Fisher Mg(OH)₂ FCC/USP is included for each technique, for comparison purposes. The manufacturer claims an LOI on this material of 30.2 % (Fisher Chemical, 2005) under the same temperature protocol that is described in Subsection B2 of Appendix B; however the manufacturer does not give an associated uncertainty for this number. In cells A21-B22 the average and standard deviation of both the TGA and LOI experiments (combined) are calculated.

In cells A24 through C36, the molecular weights of all possible phases (compounds, elements) are calculated. Column A gives the molecular formula, column B gives the mineral name, and column C gives the molecular weight in (g/mol).

In cells A40 through Y42, Equations 1-7 are solved along with propagation of uncertainty. Row 41 contains the results on the mean values, and row 42 contains the uncertainty. Cell B41 is calculated using Equation 6, cell B42 is calculated using Equation 14. Cells C41-D42 show the amount of lime and are self explanatory. Cell E41 is calculated from Equation 5 and uncertainty in E42 is calculated using Equation 9. Cells F40-L42 are self explanatory. In cells M40 through P42 we use Equations 1-2, and assign $x_i = 0$ for the other phases. Uncertainty is propagated using Equation 9. Cells Q40-S42 are self explanatory. Cell T41 is calculated using the numerator of Equation 7. Uncertainty is propagated in cell T42 using Equation 13. Cell U41 then completes Equation 7 and uncertainty is propagated cell U42 using Equation 13. Then the total moles/g sample is summed in cell V41, with uncertainty in V42 (which isn't used) from Equation 13. The mole fractions of periclase and lime are given in cells W41 and X41 respectively, using Equations 3 and 4. The uncertainty in these cells is calculated in W42 and X42 using Equation 15. The sum is calculated in Y41 and the uncertainty in Y42 using Equation 13.

APPENDIX B. EXPERIMENTAL PROTOCOL

B.1 Dissolution of MM MgO in Nitric Acid

Below is an overview of the procedure used to dissolve MM MgO in nitric acid. The resulting liquid is then analyzed by the ICP-AES. The exact procedure for each sample is located in the scientific notebook:

Prepare solution A: MgO HNO₃ solution for Ca, Al, Fe, Si analysis:

- 1) Grind the 5-6 g of MgO sample by mortar and pestle.
- 2) Weigh out 1g (0.9-1.1g) of the ground sample into a 100 ml volumetric flask
- 3) Rinse the volumetric flask with 40-50 ml DI water and make sure all the sample is washed into the volumetric flask.
- 4) Add 9 ml of concentrated HNO₃ into the flask.
- 5) Pipette 100ul of 1000ppm Sc standard into the flask.
- 6) Add DI water in the flask until the meniscus is at the 100 ml line.
- 7) Shake the flask well.
- 8) Most of the MgO sample will be dissolved by the nitric acid. But some black particles are not dissolvable (most likely spinel see Subsection 3.4). Let the MgO sample-HNO₃ solution settle for 2-3 hr, the black particles may be observed at the bottom of the flask.

Prepare Solution B: MgO HNO₃ solution for Mg²⁺ analysis:

- 1) Pipette 1000ul of the top clear solution from solution A into a 100ml volumetric flask.
- 2) Rinse the volumetric flask with 40-50 ml DI water and make sure all the MgO sample-HNO₃ solution is washed into the volumetric flask.
- 3) Pipette 5000ul of concentrated HNO₃ into the flask. Add the HNO₃ slowly with continuous swirling.
- 4) Pipette 100ul of 1000ppm Sc standard into the flask.
- 5) Add DI water in the flask until the meniscus is at the 100 ml line.

- 6) Shake the flask well.

B.2 TGA and LOI Analysis

Below is an overview of the procedure used to prepare and analyze samples for TGA and LOI analysis. The exact procedure(s) for each sample are located in the scientific notebooks.

For the sample set labeled 90-922-1 through 90-922-4 (see APPENDIX A for location of data in spreadsheet), the samples were prepared for TGA and LOI analysis as follows (see pp 97-98 of scientific notebook WIPP-MM MgO-2):

- 1) 6-7 grams of MM MgO sample were loaded into clean 125 ml plastic bottles.
- 2) 100 ml of de-ionized water was added.
- 3) The threads of the bottles were covered in Teflon tape.
- 4) The bottles were closed and placed into a 90°C oven.
- 5) The bottles were placed in the oven on 9/22/06. Samples 90-922-3 and 4 were removed on 9/26/06. Samples 90-922-1 and 2 were removed on 9/28/06. The difference in TGA results from these two collection dates does not appear to be significant (see Microsoft Excel spreadsheet 90-922 results 4.xls).
- 6) Upon removing from the oven the samples were rinsed, filtered and dried in air overnight.

The dried-hydrated MM MgO sample was then analyzed by TGA in a Netzsch STA 409 PC TGA/DTA DSC under argon that has been filtered for oxygen and water, and in parallel in a Fisher Programmable furnace, in air. In the TGA (which measures weight loss continuously) the temperature program was as follows:

- 1) Heat to 150 °C at 6 °C/min, remain at 150 °C for 2 hours.
- 2) Heat to 800 °C at 3 °C/min, remain at 800 °C for 15 minutes.

In the Fisher Programmable furnace, the temperature program was as follows:

- 1) Heat to 150 °C, remain at 150 °C for 2 hours.
- 2) Remove sample from oven, allow to cool (for a short time ~ ½ hour), then measure weight loss.

- 3) Heat to 800 °C at 4 °C/min, allow oven to cool, remove sample from oven, allow sample to cool (~ 1 hour), then measure weight loss.

This program is the same as used by Fisher Chemical to analyze their FCC/USP magnesium hydroxide (Fisher Chemical, 2005).

Information Only



Chavez, Mario Joseph

From: Roselle, Gregory Thomas
Sent: Tuesday, August 07, 2007 4:25 PM
To: Chavez, Mario Joseph
Cc: Deng, Haoran
Subject: MgO Milestone report

Mario,

I give you signature authority for subject document. I have completed my Technical review and Haoran has my completed DRC.

Greg

Information Only

8/8/2007